(B) Texture

in german: Textur = Sedimentgefüge (dagegen: Struktur = Sedimentstrukturen

1. Grain size
2. Grain morphology (shape, roundness, surface texture, etc.)
3. Sorting (grain-size distribution)
4. Grain fabric (packing, contacts, orientation)

1) see script p. 5

2) Grain morphology

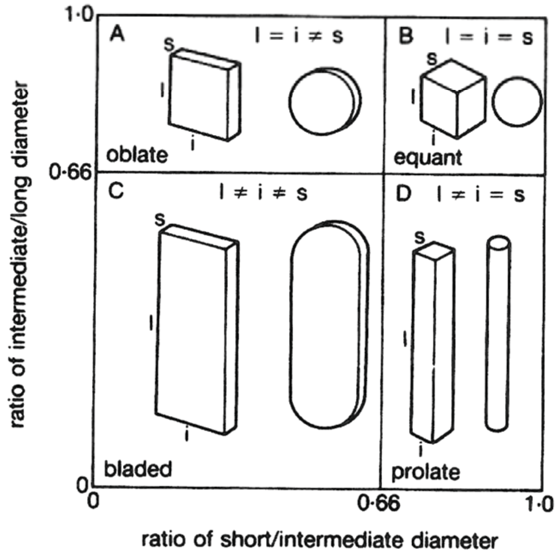

Fig. 2.5 The four classes of grain shape based on the ratios of the long (l), intermediate (i) and short (s) diameters (after T. Zingg). Classes are A, oblate (tabular or disc-shaped); B, equant (cubic or spherical); C, bladed and D, prolate (rod-shaped). For each class a shape is illustrated of roundness 0 and 6 (see Fig. 2.6).

Tucker 1991

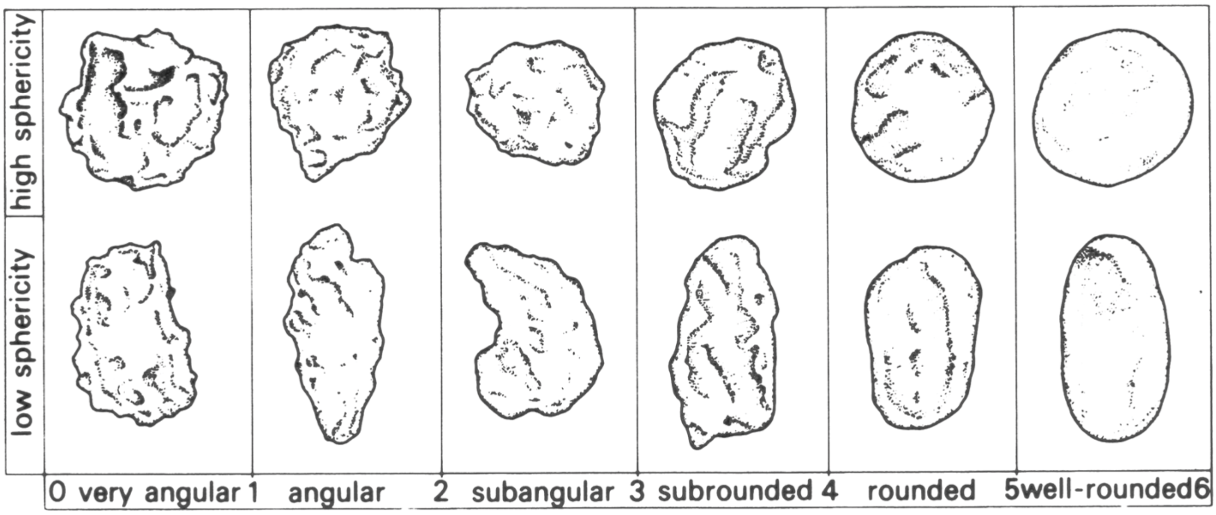

Tucker 1991 p.16

Fig. 2.6 Categories of roundness for sediment grains. For each category a grain of low and high sphericity is shown. After Pettijohn *et al.* (1987)

Flügel 1978 p.173

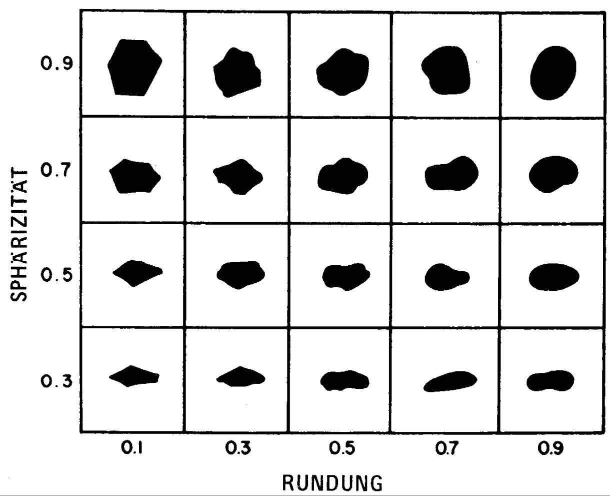

Abb. 31 Schätzbilder für Rundung und Sphärizität. Nach Krumbein u. Sloss (1963). Erforderlich ist die Erfassung von mindestens 100 Komponenten, wobei unterschiedliche Korngrößenklassen zu berücksichtigen sind.

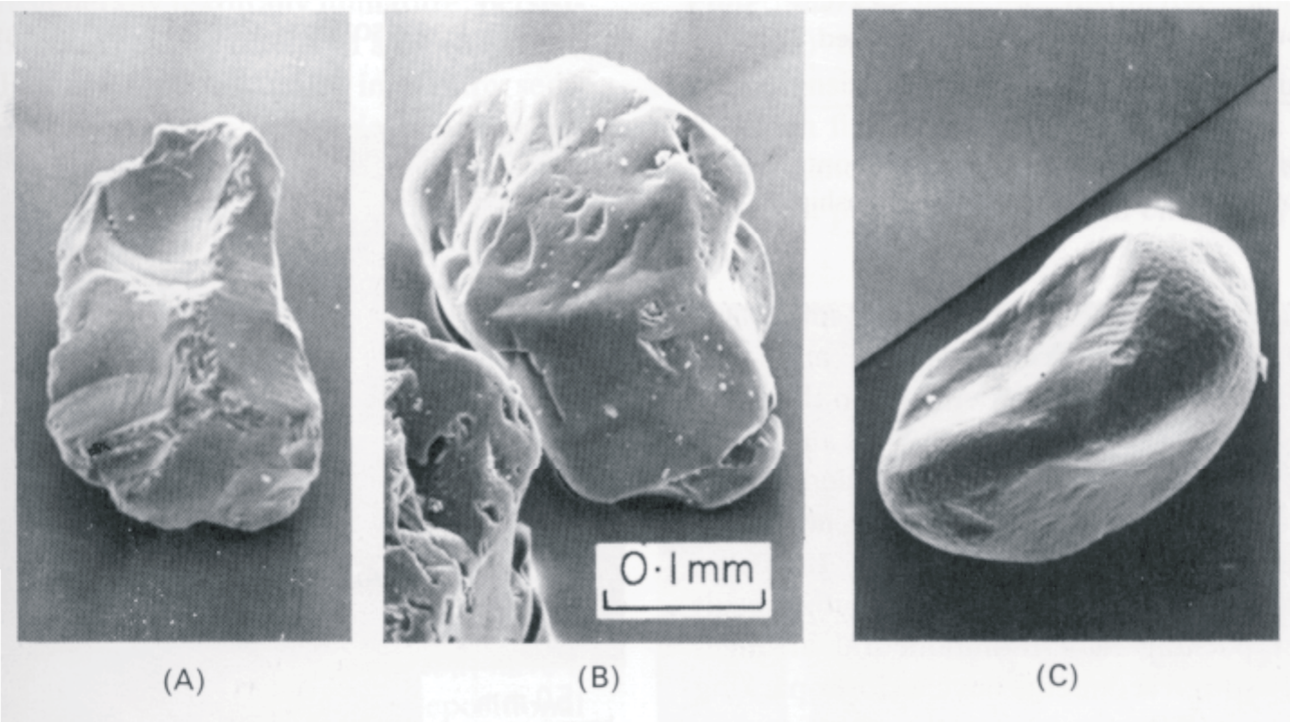

SEM images of quartz grains: (A) glacial, (B) hifh-energy beach , (C) aeolian

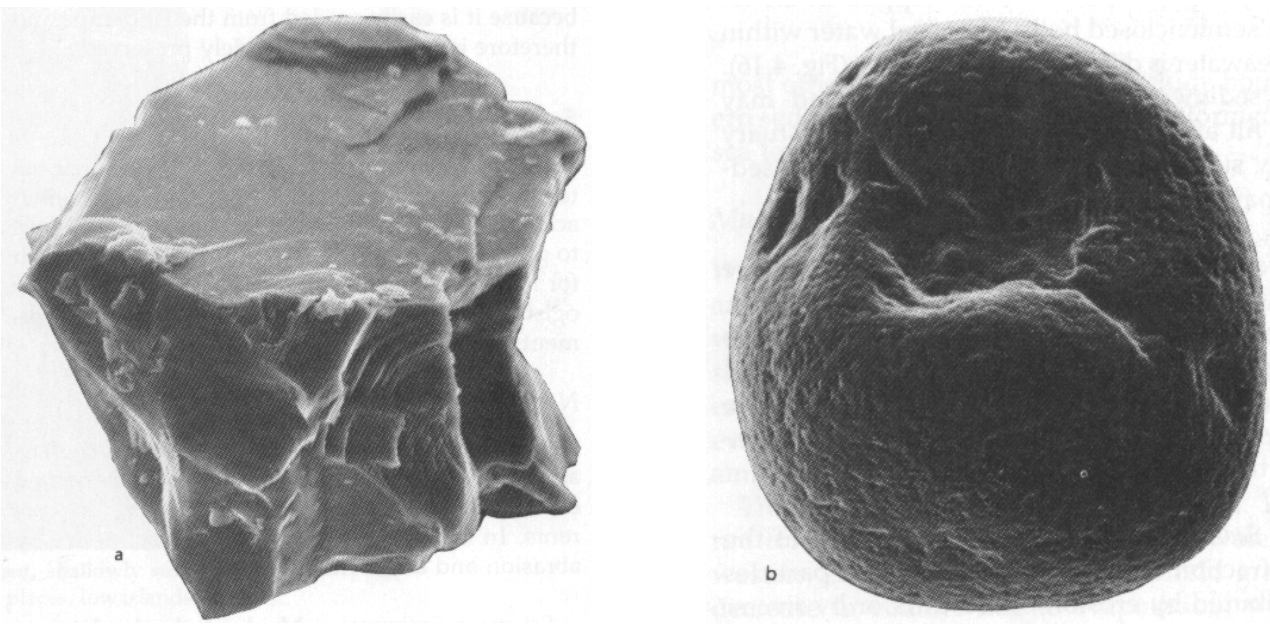

FIGURE 4.18 Surface features of sand grains, seen on enlarged pictures taken with a scanning electron microscope, aid in differentiating among transporting agencies. (a) Surface of a quartz grain (0.1-mm diameter) that has been crushed and abraded during transport at the bed of a Swiss glacier displays distinctive concoidal fractures. (b) Surface of a wind-transported quartz grain (0.5-mm diameter) from south-central Libya has a distinctive pitted appearance caused by mechanical chipping as grains impact one another during strong sandstorms.

Skinner & Porter 1989

zu 3) Sorting

Fig. 2.3 Formulae for the method of moments for grain-size analyses, f is the percentage fraction in each class interval of the total weight of sediment (if a sieve analysis) or of the total number of grains (if data from a thin section), and $m\phi$ is the mid-point value of each class interval in phi units

Tucker 1991 p.13/14

Mean (first moment) $= \bar{x} = (f_1 m\phi_1 + f_2 m\phi_2 \ldots + f_n m\phi_n)/100$, i.e. $\dfrac{\Sigma f m\phi}{100}$

Standard deviation (second moment) $= \sigma$

$$= \sqrt{\frac{f_1(m\phi_1 - \bar{x})^2 + f_2(m\phi_2 - \bar{x})^2 \ldots + f_n(m\phi_n - \bar{x})^2}{100}},$$

i.e. $\sqrt{\dfrac{\Sigma f(m\phi - \bar{x})^2}{100}}$

Moment coefficient of skewness $= \alpha_3 = \dfrac{\Sigma f(m\phi - \bar{x})^3}{100\sigma^3}$

Mean-cubed deviation $= \alpha_3\sigma^3 = \dfrac{\Sigma f(m\phi - \bar{x})^3}{100}$

Tucker 1991
S.14

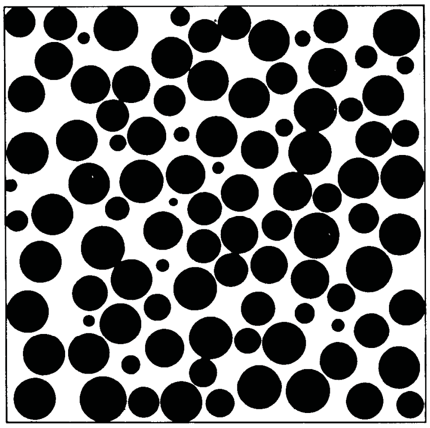

Fig. 2.3 Random section through spherical grains of equal size, showing the apparent diffrent grain sizes present.
The view has an apparent sorting of 0.58 (i.e. moderately well sorted) whereas the true sorting value is 0 (i.e. very well sorted).
Reproduced from Harrell (1984) with permission of the Society of Economic Paleontologists and Mineralogists.

Sorting:
(σ = standard deviation)

< 0.35	very good
0.35 – 0.5	good
0.5 – 1.0	moderate
1.0 – 2.0	poor
> 2.0	very poor

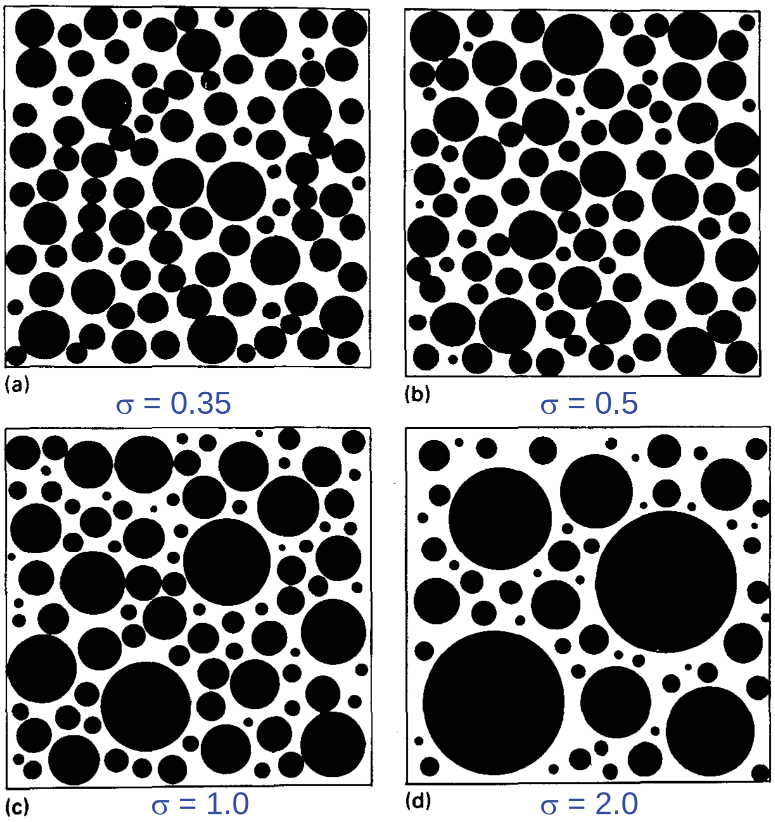

Tucker 1991 p.13/14

Fig. 2.4 Visual comparators for random sections through log-normally distributed sets of spherical grains. Actual sorting in (a) is 0.35, in (b) 0.5, in (c) 1.00 and in (d) 2.00. Apparent sorting is 0.69, 0.77, 1.16 and 2.08 respectively. Note that the disparity is greater for very well sorted grains (a), than for the less well sorted (c and d). Reproduced from Harrell (1984) with permission of the Society of Economic Paleontologists and Mineralogists.

zu 4) Grain fabric

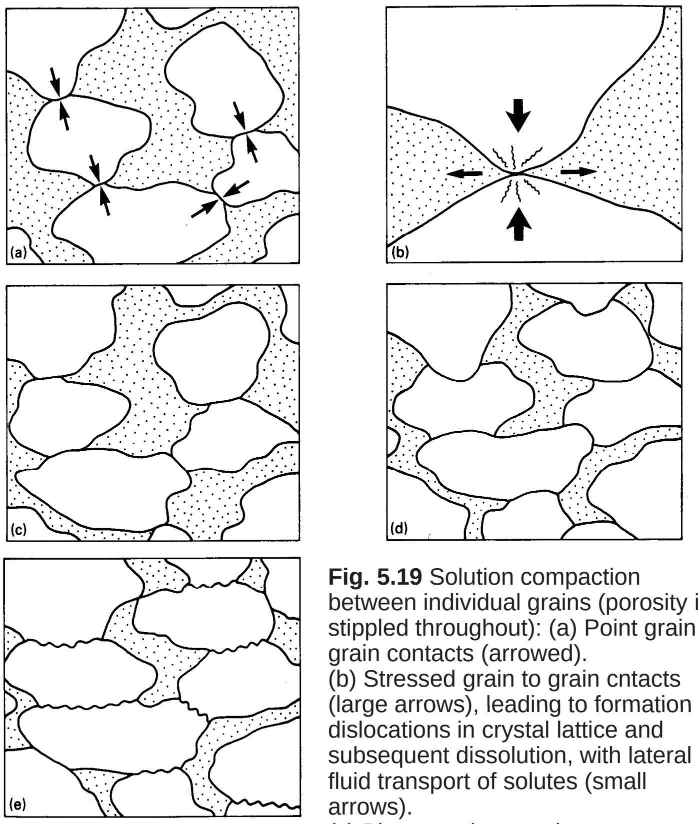

Tucker 1988 p.131

Fig. 5.19 Solution compaction between individual grains (porosity is stippled throughout): (a) Point grain to grain contacts (arrowed).
(b) Stressed grain to grain cntacts (large arrows), leading to formation of dislocations in crystal lattice and subsequent dissolution, with lateral fluid transport of solutes (small arrows).
(c) Planar grain to grain contacts.
(d) Interpenetrating grain to grain contacts.
(e) Sutural grain to grain contacts.

Pettijohn et al. 1987 p.85

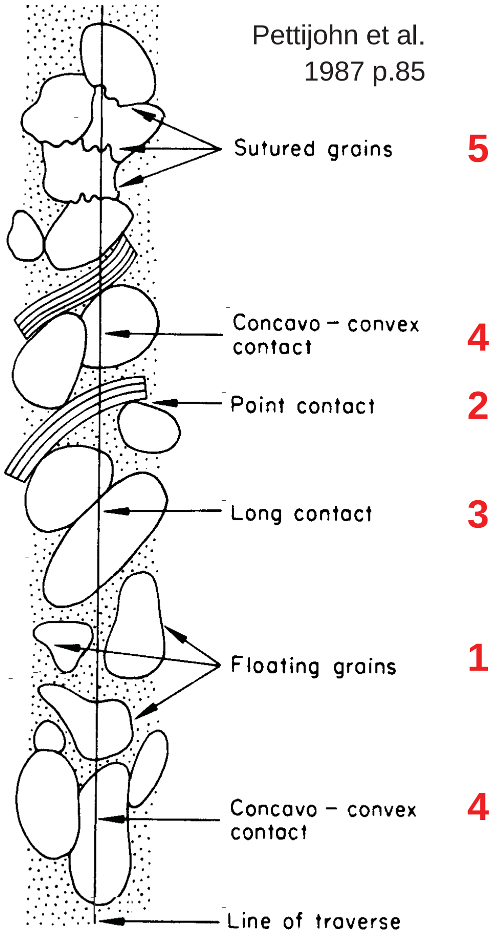

Fig. 3-11 Definition sketch of fabric terminology: quartz (white), mica (lined) and matrix (stippled).

(C) Classification (nomenclature)

McBride (1963)

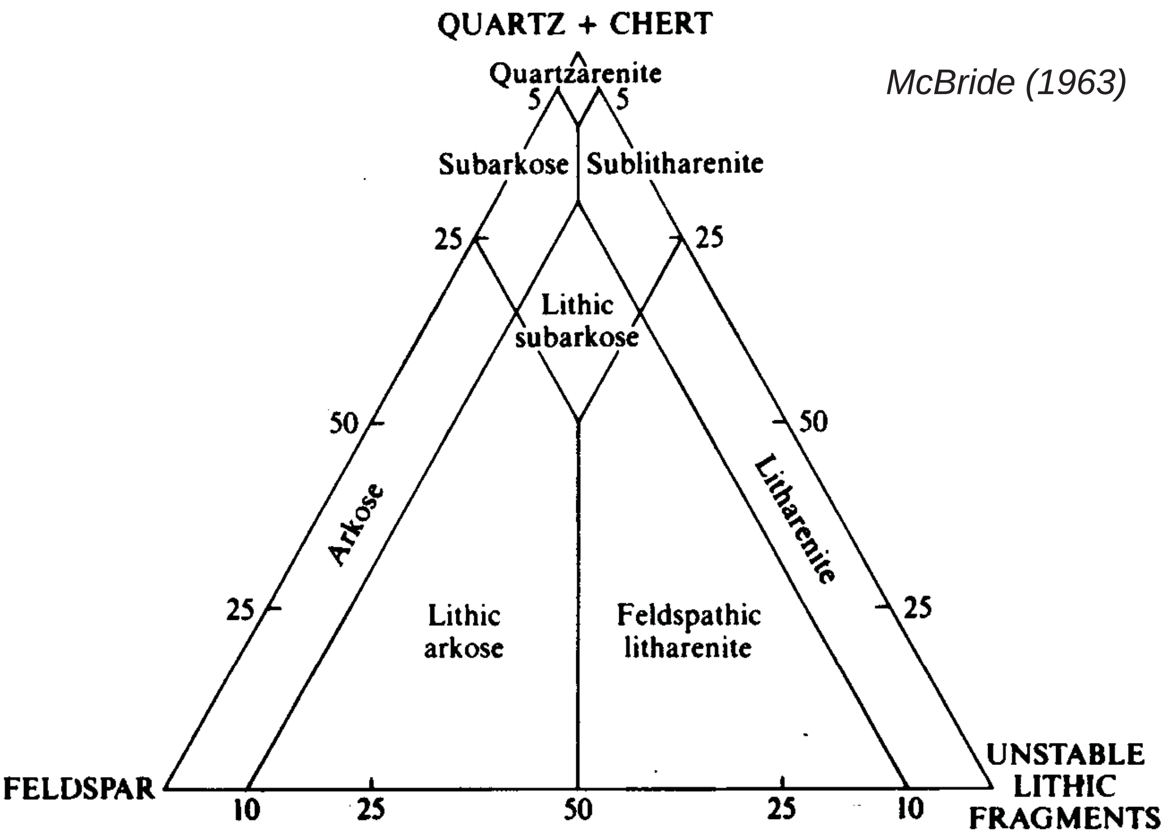

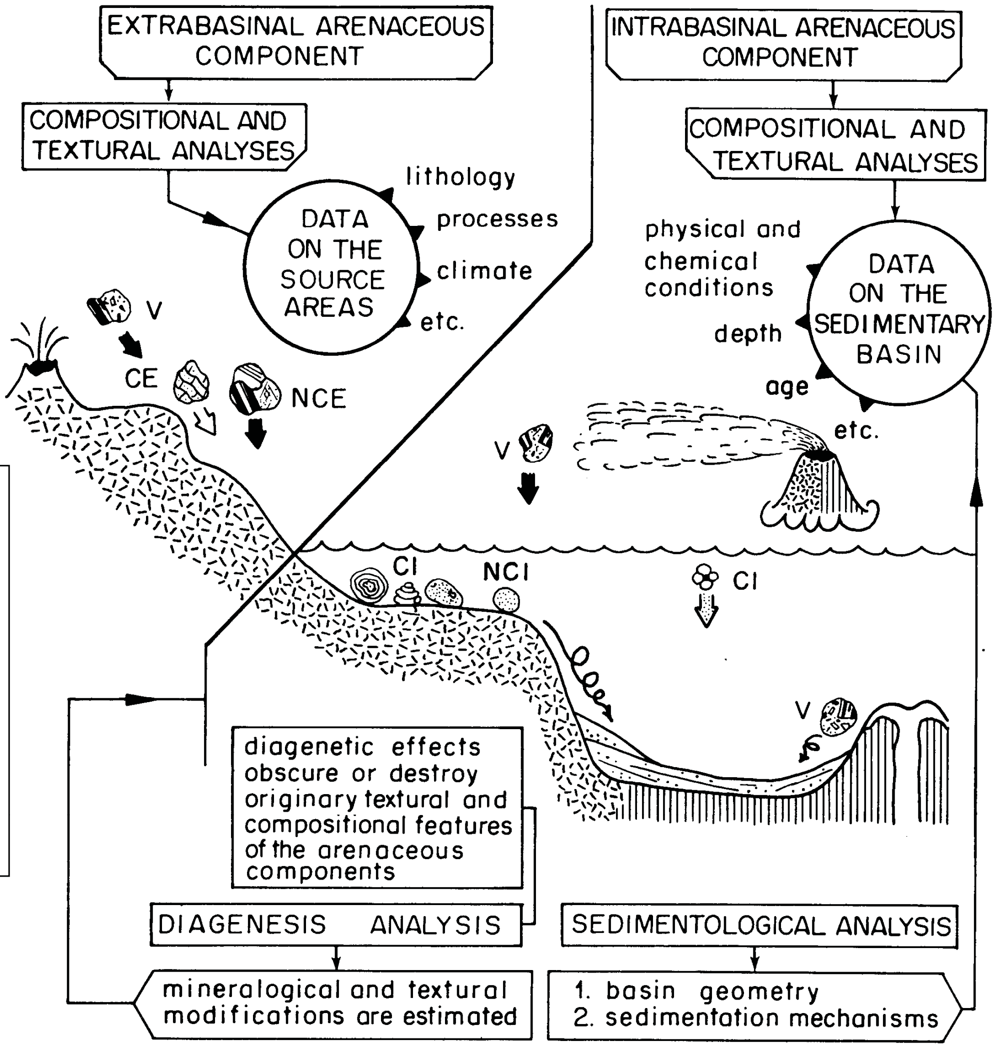

Fig. 1.– Schematic relationship between arenaceous components and data provided by the optical and sedimentological analyses of a marine arenite. NCE: noncarbonate extrabasinal grains; CE: carbonate extrabasinal grains; NCI: noncarbonate intrabasinal grains; CI: carbonate intrabasinal grains; V: volcanic grains.

Zuffa 1980 p.23

Fig. 3.– Main types of arenites as defined by optical analysis of the arenaceous modes.

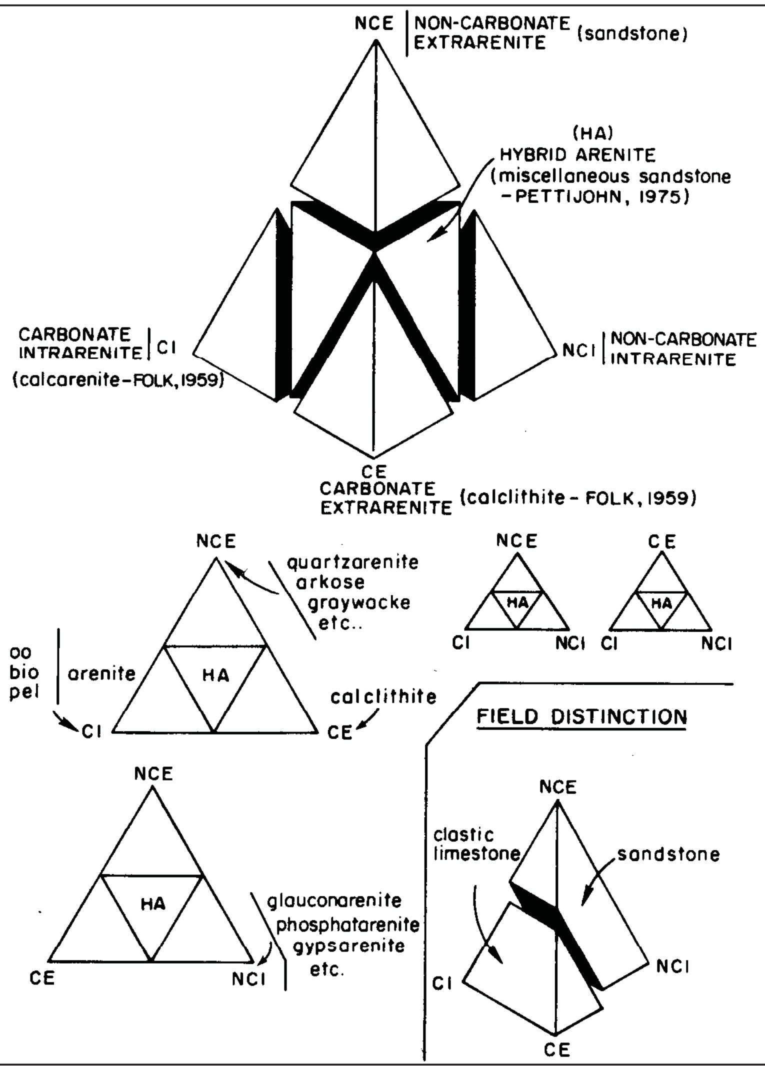

Zuffa 1980 p.25

First order classification

2nd order classification

McBride 1963

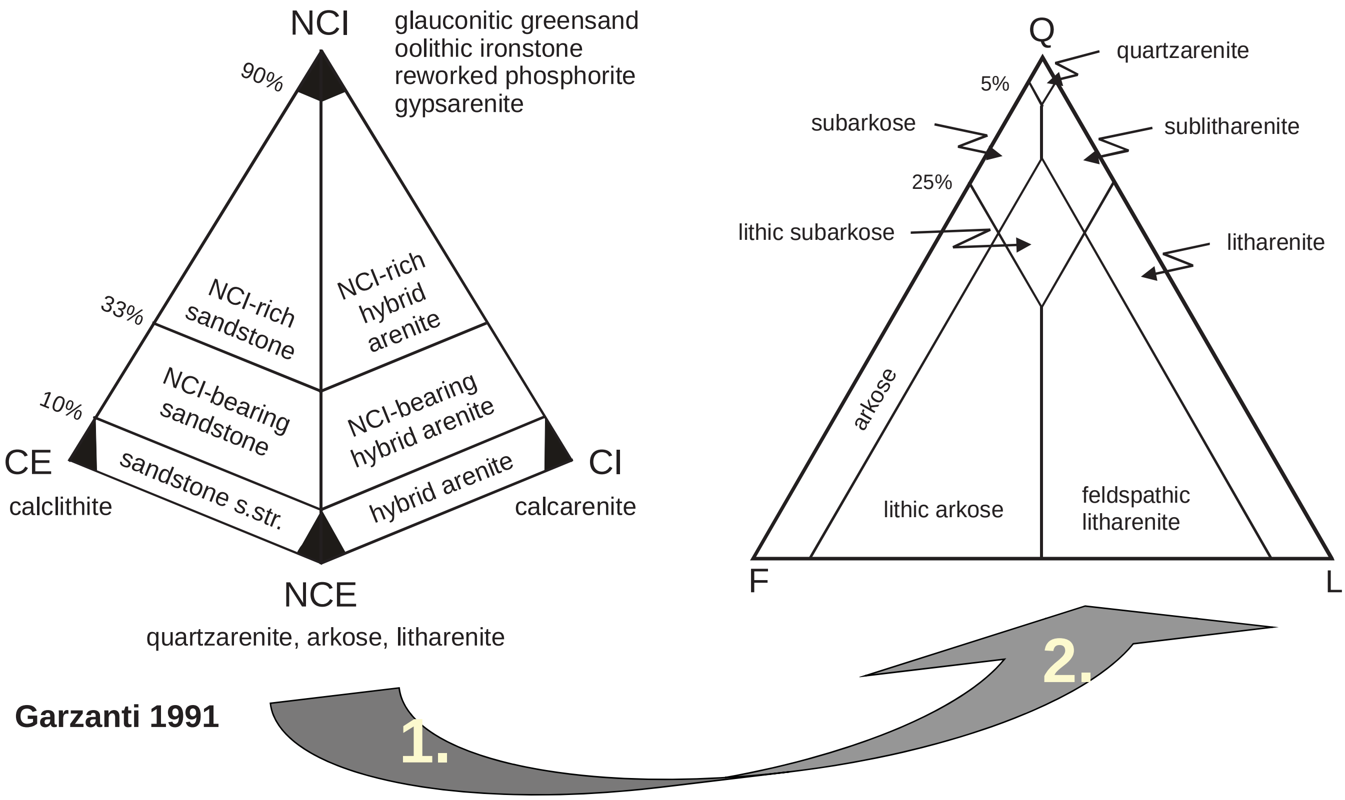

(modifiziert nach Garzanti 1991 und McBride 1963)

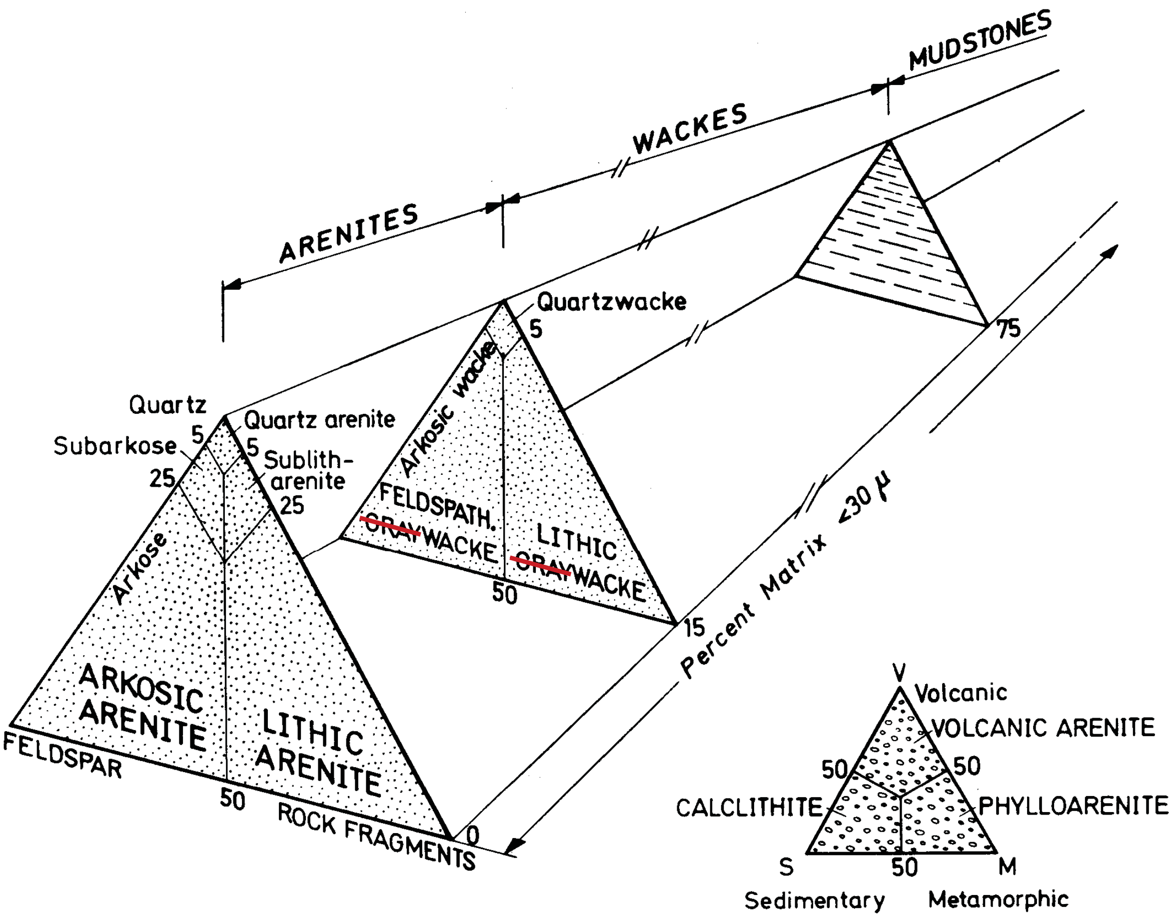

Fig. 5-1 Classification of terrigenous and sandstones (Modified from Dott. 1964. Fig. 3)

Pettijohn et al. 1987 p.145

Quantification of the framework constituents (components)

Why?

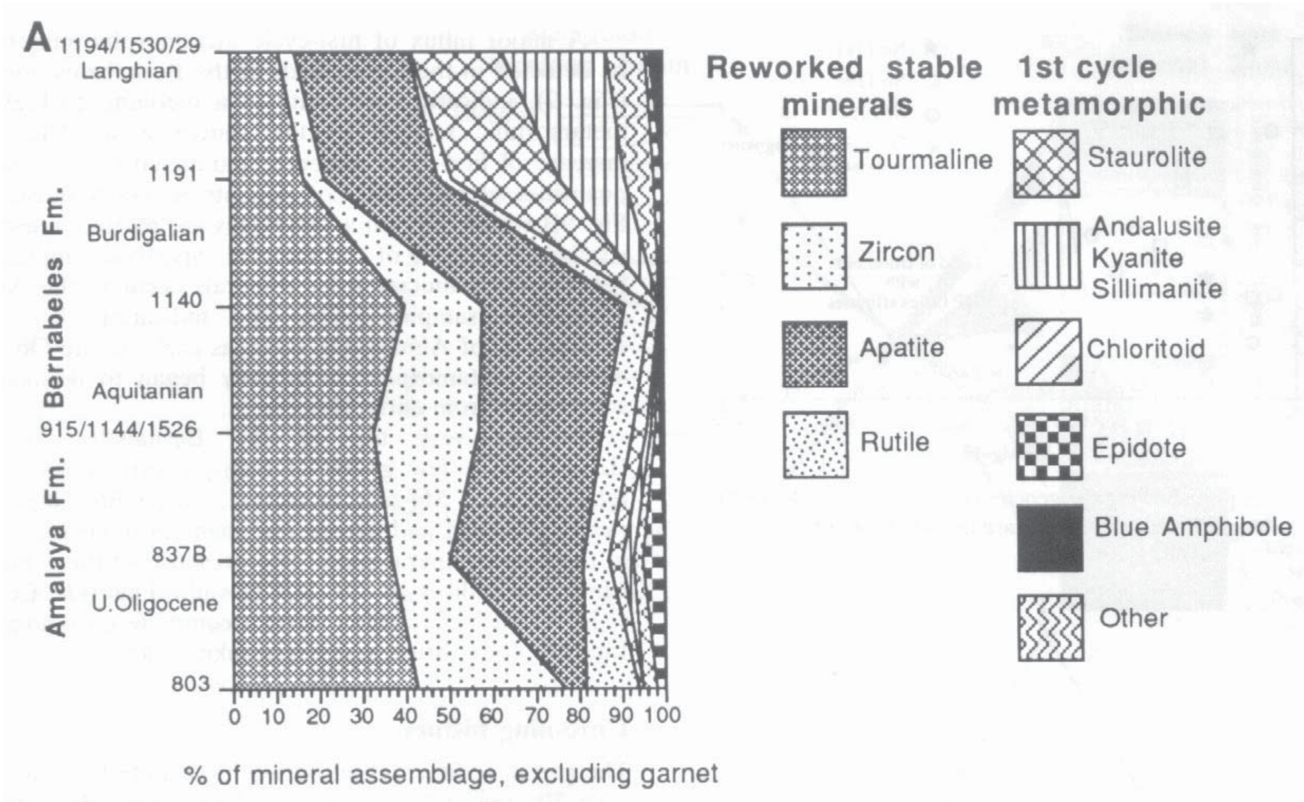

Quantification of the framework constituents (components)

percentage composition of the sediment components

→ **modal composition**

<u>1) quantitative:</u> point-counting techniques, special oculars (grid)

<u>2) semi quantitative:</u> estimation techniques, frequency classes

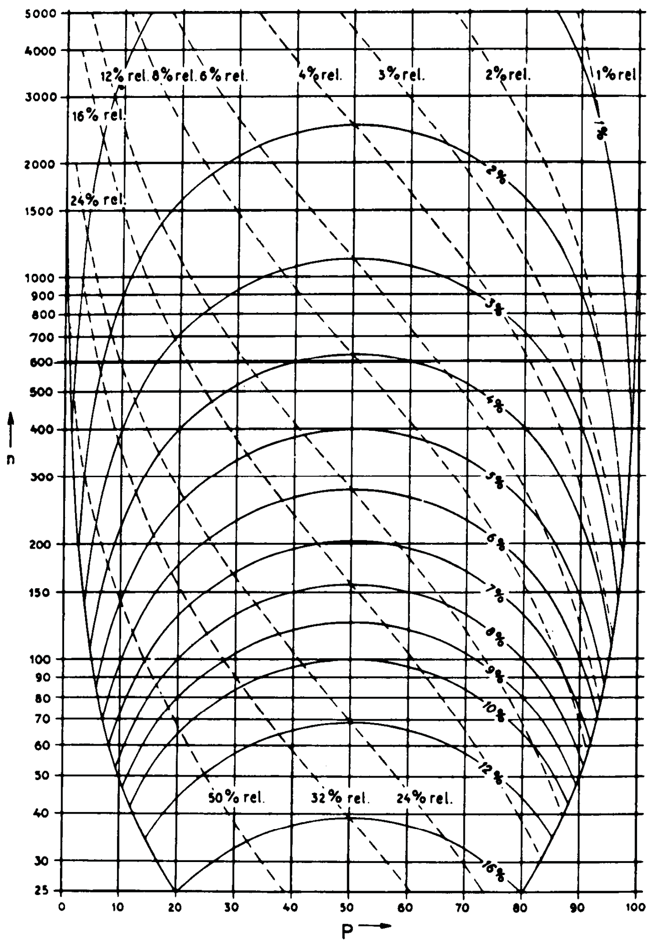

Abb. 24. Schätzung der statistischen Wahrscheinlichkeit von Zählungen nach dem Point-Counter-Verfahren (nach Plaas u. Tobi, 1965). Es bedeuten: *n*, Gesamtanzahl der Treffer; *P*, Prozentsatz, mit welchem ein Element (z.B. Ooide) im Schliff auftritt. Die Wahrscheinlichkeit kann durch die Standardabweichung angegeben und damit der tatsächliche Gehalt des Elementes (p) in Vol.% geschätzt werden. *Durchgezogene Linie*, absoluter Fehler; *strichlierte Linie*, relativer Fehler

aus: **Flügel 1978 S.153** (Mikrofazielle Untersuchungsmethoden von Kalken; engl. Version available, 1982)

Tab. 3.1: Absoluter Fehler in % in Abhängigkeit von der Anzahl der ausgezählten Körner n und der Häufigkeit eines Korntyps p. Berechnet nach $s = \sqrt{[p(100-p)/n]}$ (VAN DER PLAS & TOBI 1965). Der angegebene Fehler beträgt 2s (95%ige Wahrscheinlichkeit).

n / p	100	200	300	600
5%	4.4	3.1	**2.5**	1.8
10%	6.0	4.2	**3.5**	2.5
20%	8.0	5.7	**4.6**	3.3
40%	9.8	6.9	**5.7**	4.0

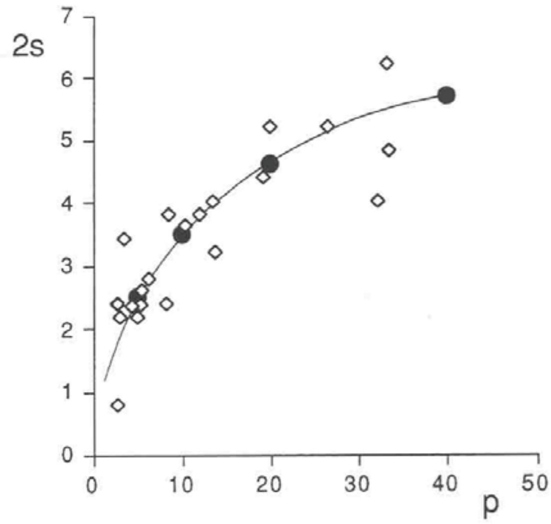

Abb. 3.3:
Verhältnis der Standardabweichung (2s) zur Häufigkeit eines Korntyps in % (p). Kurve und schwarze Kreissignaturen zeigen die theoretischen Werte aus Tab. 3.1 für n = 300. Vierecke zeigen die ermittelten Standardabweichungen aus Tab. 3.2.

Tab. 3.2: Mittelwert m und mittlerer Fehler 2s (in Klammern, Standardabweichung einer Stichprobe, 95%ige Wahrscheinlichkeit) der häufigsten Korntypen von drei Sandsteinproben (n = 5). Die Standardabweichung wurde berechnet nach $s = \sqrt{[\Sigma(x-m)^2/(n-1)]}$ (GRÄNICHER 1994: S.3-10).

Probe	Q_m	Q_p	Q_c	L_m	C_m	C_s	D
H 1021-5	19.2 (4.4)	13.2 (3.9)	5.5 (2.5)	13.8 (3.2)	9.9 (3.7)	20.1 (5.2)	6.2 (2.8)
EY 4-3	5.1 (2.1)	3.6 (3.4)	5.2 (2.4)	4.3 (2.5)	33.2 (6.1)	32.2 (4.0)	8.6 (3.9)
EY 9-31	2.8 (2.5)	2.9 (2.2)	2.7 (0.9)	8.2 (2.4)	33.6 (4.7)	26.4 (5.2)	12.1 (3.8)

von Eynatten 1996 S.28f.

Sketches that help to estimate the frequency of individual grain types in sedimentary rocks.

→ you will find different types of such sketches in Flügel (1978, Mikrofazielle Untersuchungsmethoden von Kalken) or its English translation from 1982

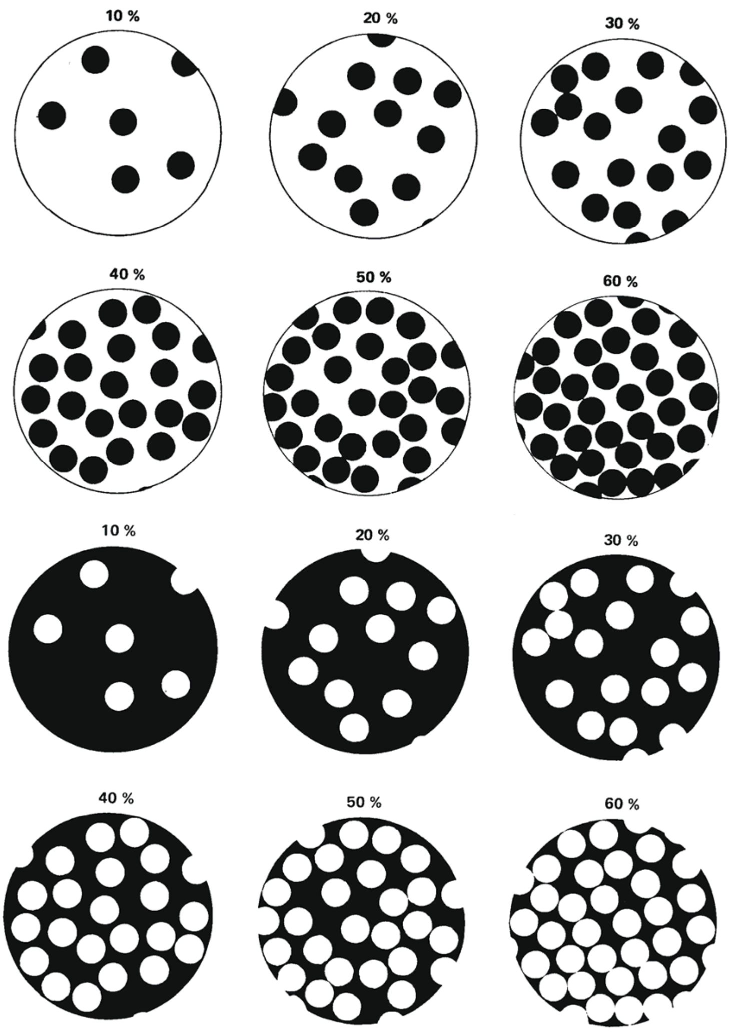

Flügel 1978 S.158

(D) Provenance-analysis

(syn.: Liefergebietsanalyse
engl.: provenance analysis)

→ Latein: „provenire“

Provenance Analysis - Approach

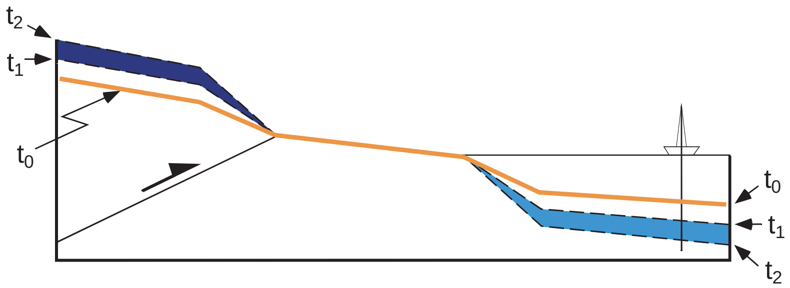

source → sediment

Modification

?

provenance model

sediment petrology
- composition
- varietal studies

chronostratigraphy

sediment dispersal

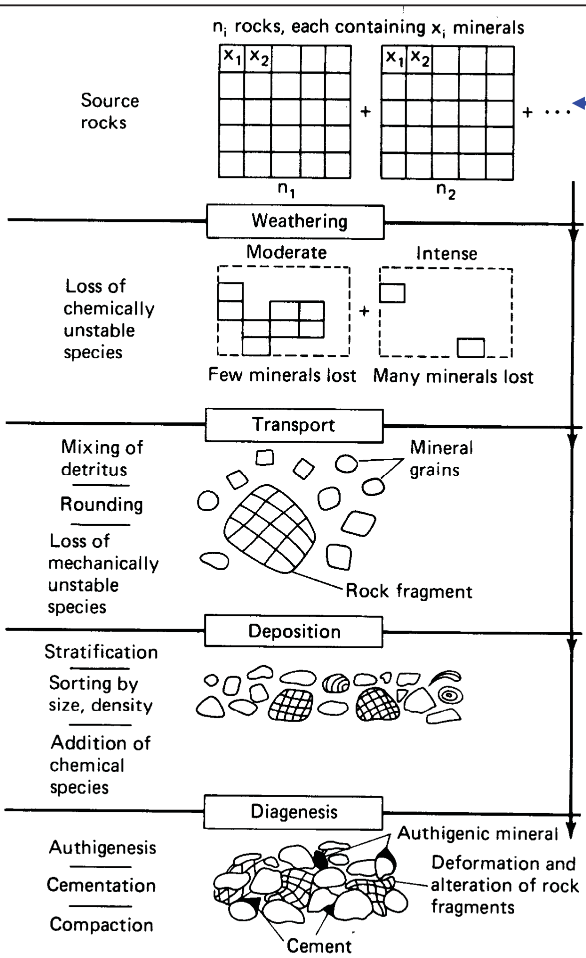

processes, that modify the potential (or initial; i.e. the composition as defined by the source rocks) composition of the sediment

Figure 2-1. The sedimentary cycle of a sandstone. Though processes such as weathering and transport are shown as distinct, they overlap in nature

Pettijohn et al. 1987

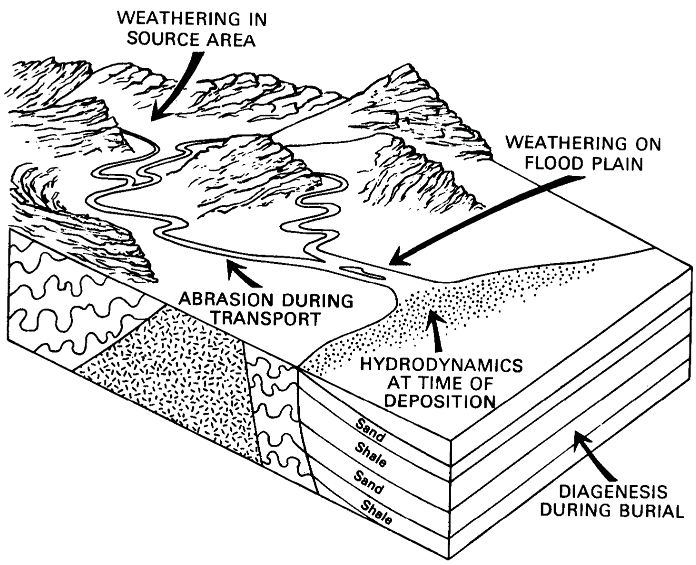

Morton & Hallsworth 1994 S.242

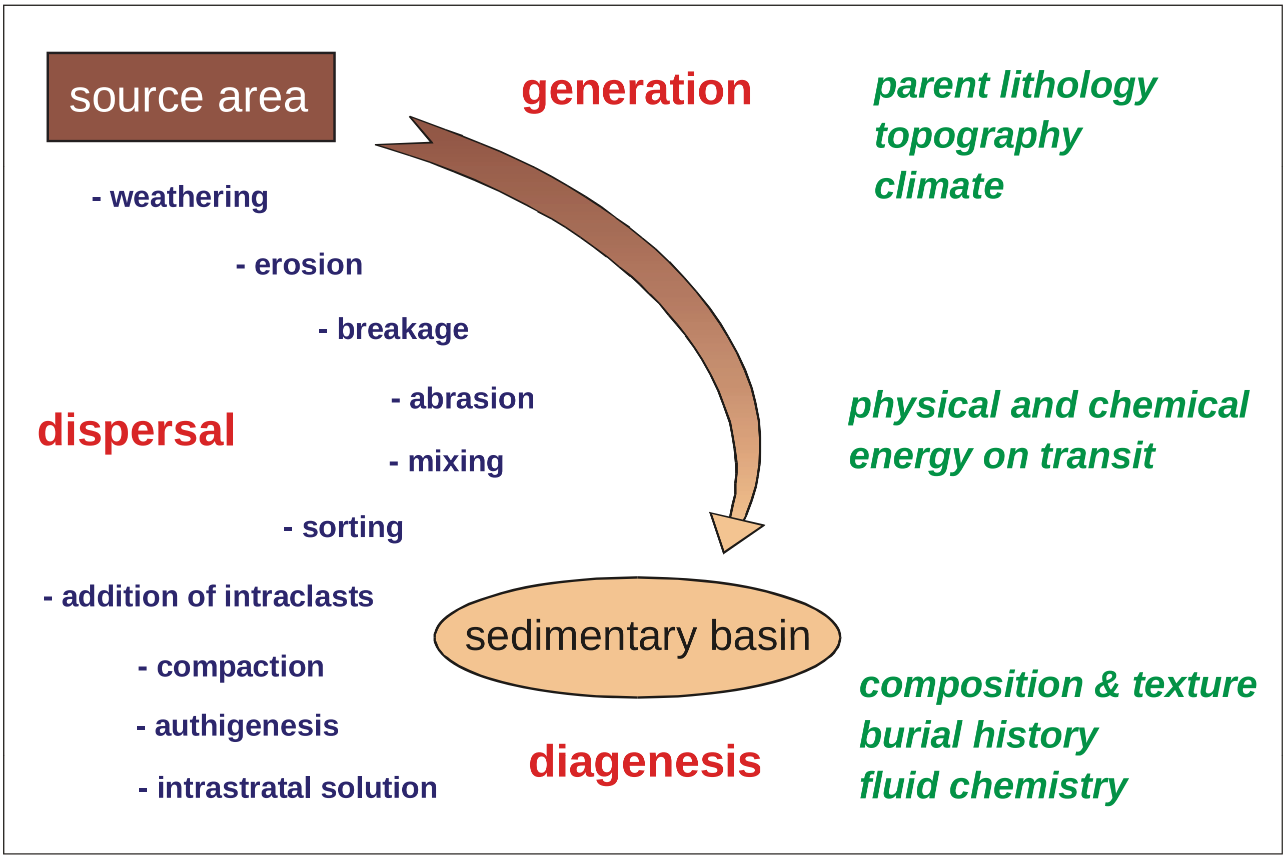

Weltje & von Eynatten 2004

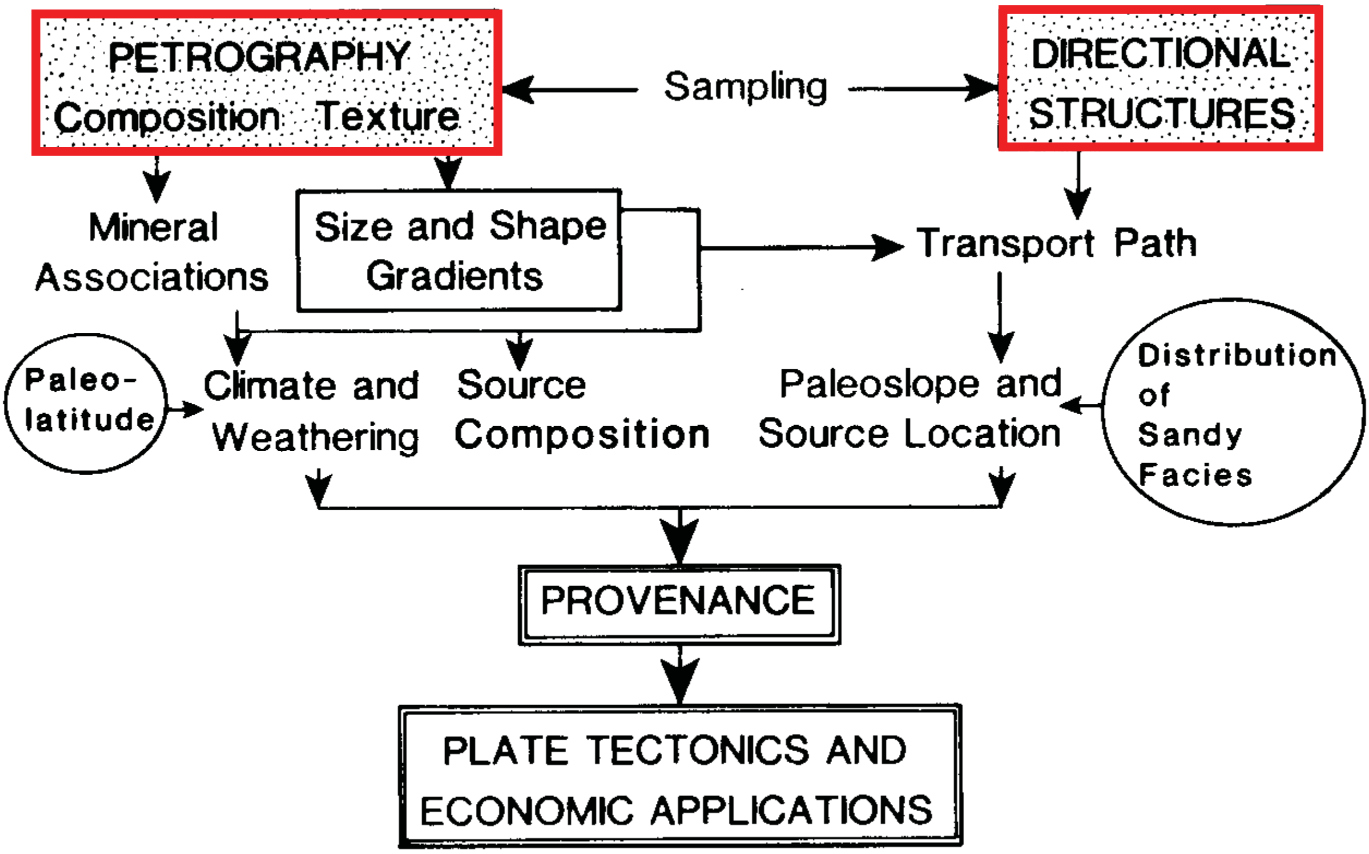

Pettijohn et al. 1987 p.264

Figure 7-5. Provenance methodology and utility. Many studies may only need to use some of these methodologies, but all are available.

HvE - Sedimentpetrologie

provenance models

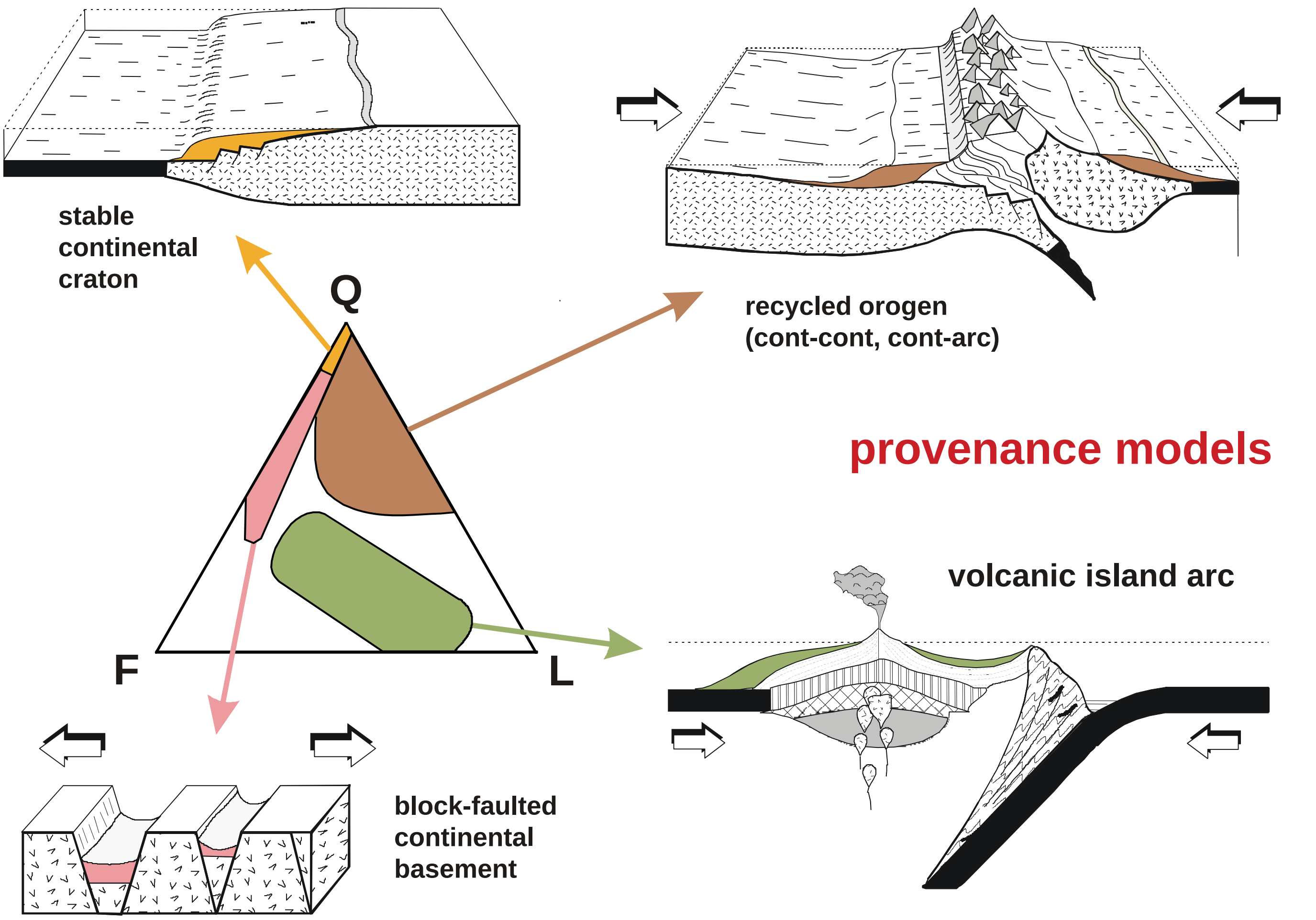

based on Dickinson 1985, modified from Fichter 2000 (http://csmres.jmu.edu/geollab/Fichter/S

„Dickinson“ model

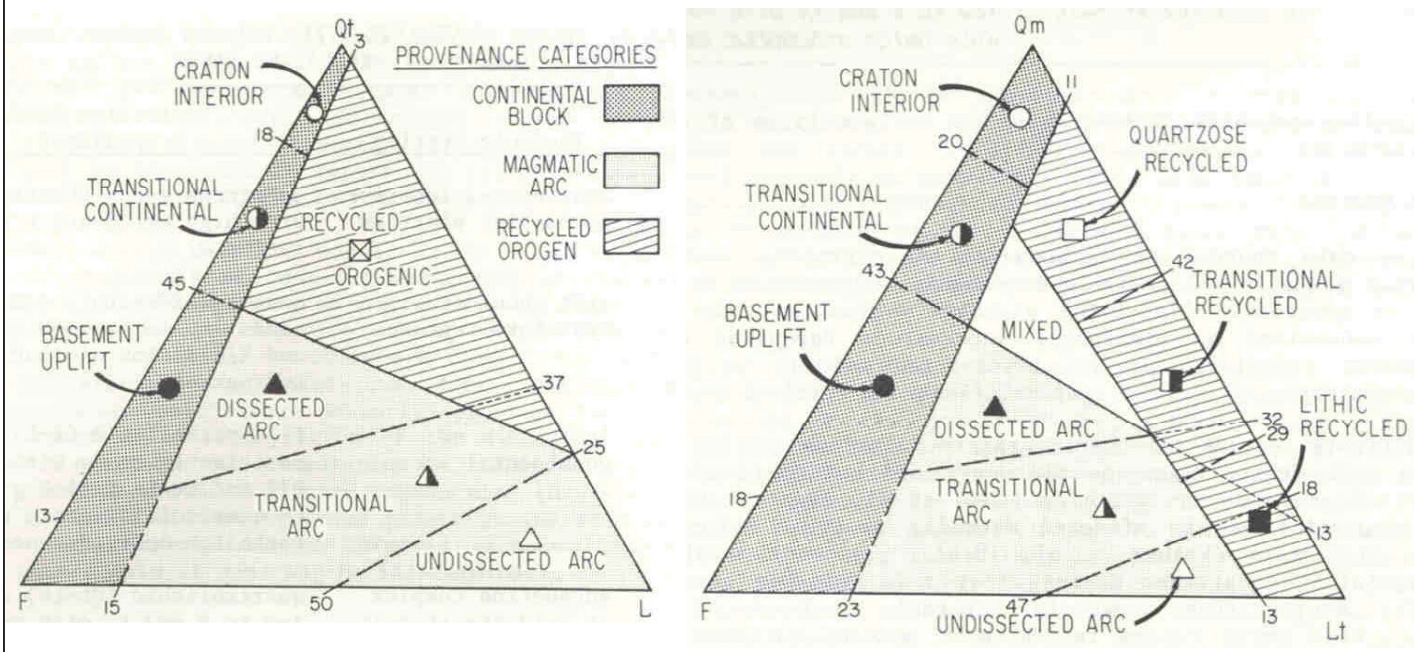

Figure 1. Provisional compositional fields indicative of sand derivation from different types of provenances (from Dickinson et al, 1983a).

Dickinson 1985

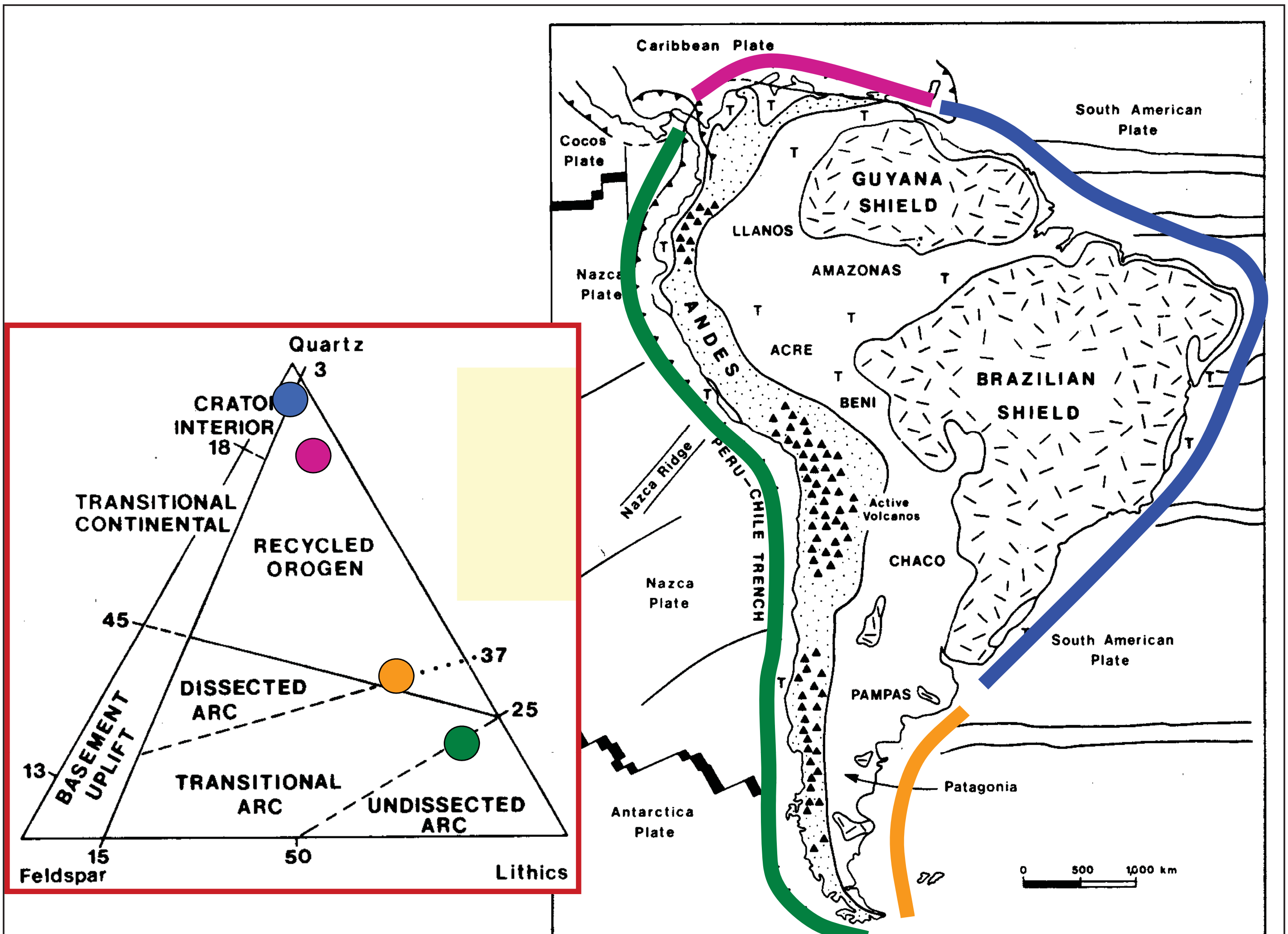

HvE - Sedimentpetrologie

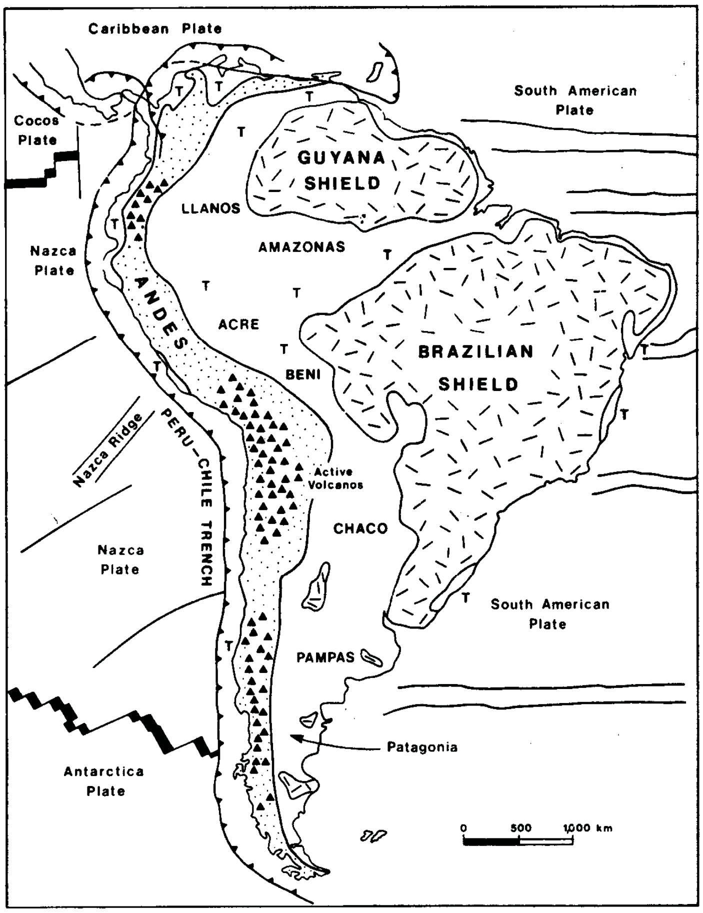

Fig. 1 Major tectonic elements of South America and adjacent ocean basins.

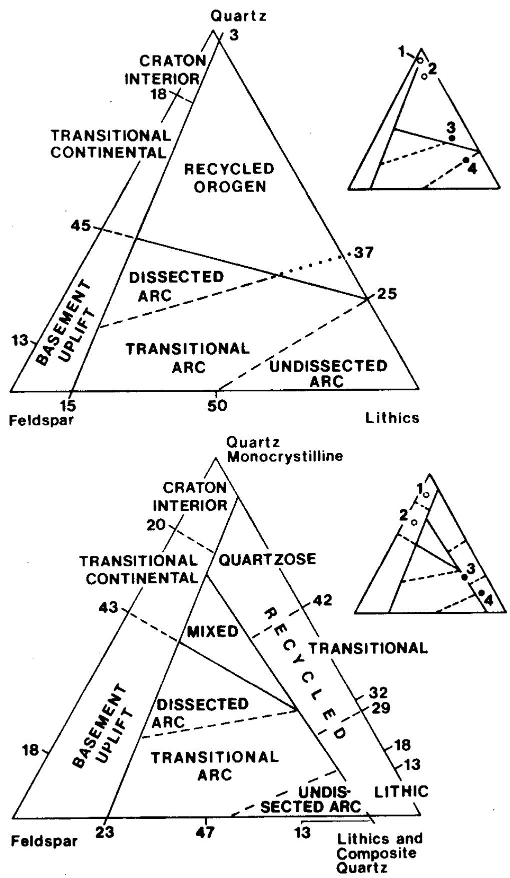

Fig. 2 Plate tectonic classification of sandstone mineralogy (after ref. 6, Fig. 1). Numbers in the small triangles indicate: 1, average composition of passive margin sands from the Rio de Plata to Trinidad; 2, beach sands from Trinidad westward along the Caribbean coast; 3, Argentine beach sands; and 4, the sands of South America's Pacific coast (see Fig. 3).

Potter 1984 p.646ff

HvE - Sedimentpetrologie

modified after
Potter 1984

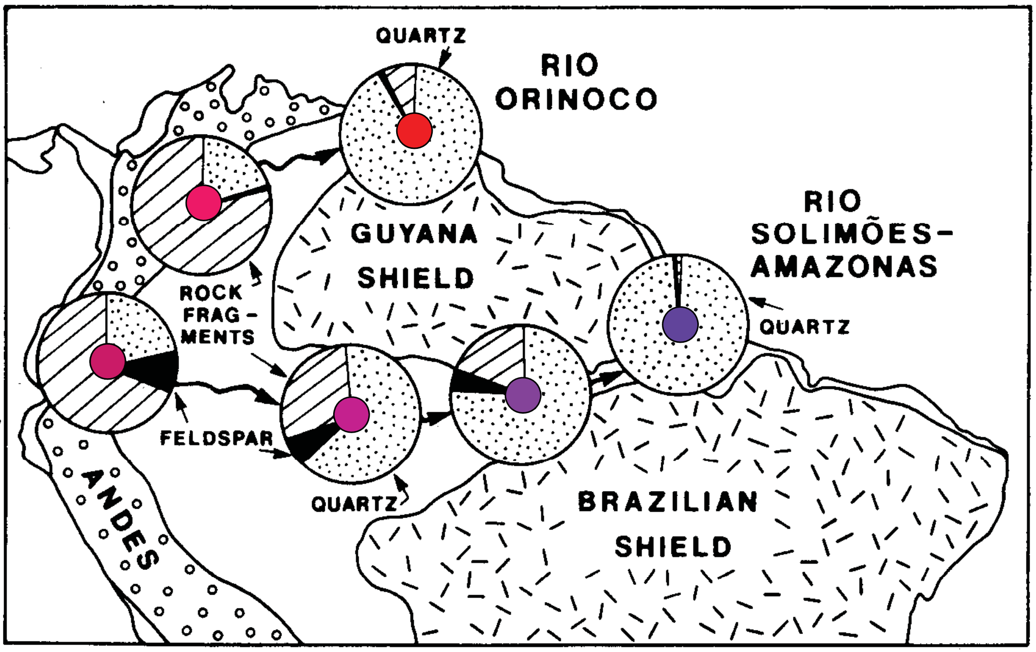

Orinoco

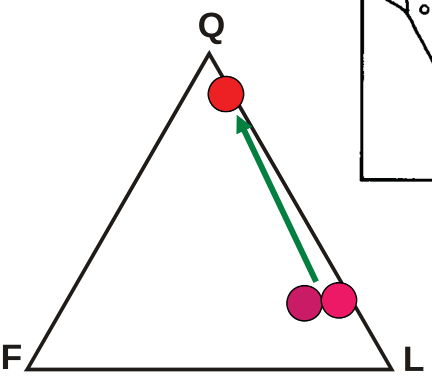

Solimões-Amazonas

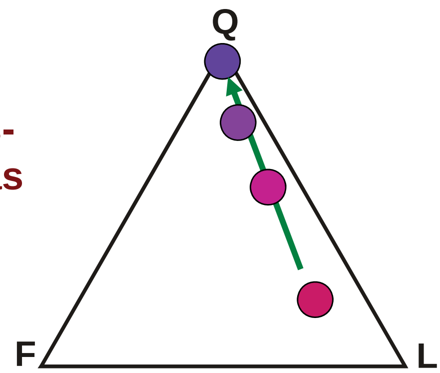

climate effect on sandstone composition

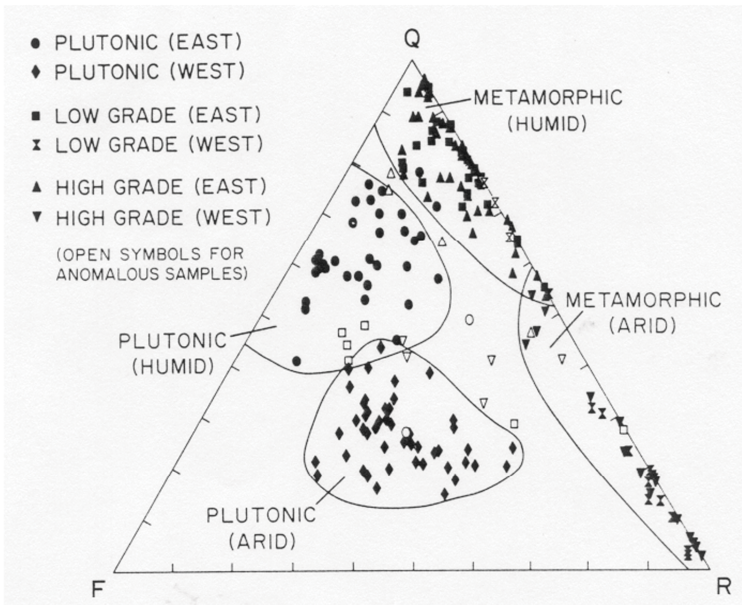

7-4. QFR ternary plot of the composition of dium-size fraction of Holocene fluvial sand -cycle parentage (from Suttner *et al.*, 1981, by permission of the Society of Economic ologists and Mineralogists).

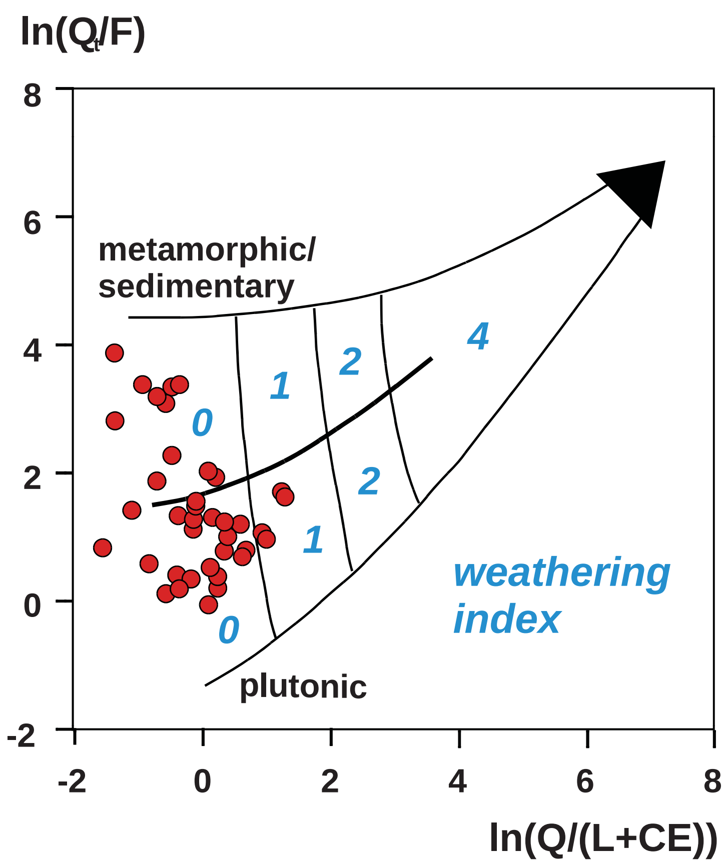

concept:

Weltje et al. 1998,
Basin Research 10

data: ●

sandstones from Swiss Molasse basin,
von Eynatten 2003,
Sedimentology 50

Case Study 1: Oligo-/Miocene foreland basin, Betic Cordillera (Lonergan & Mange

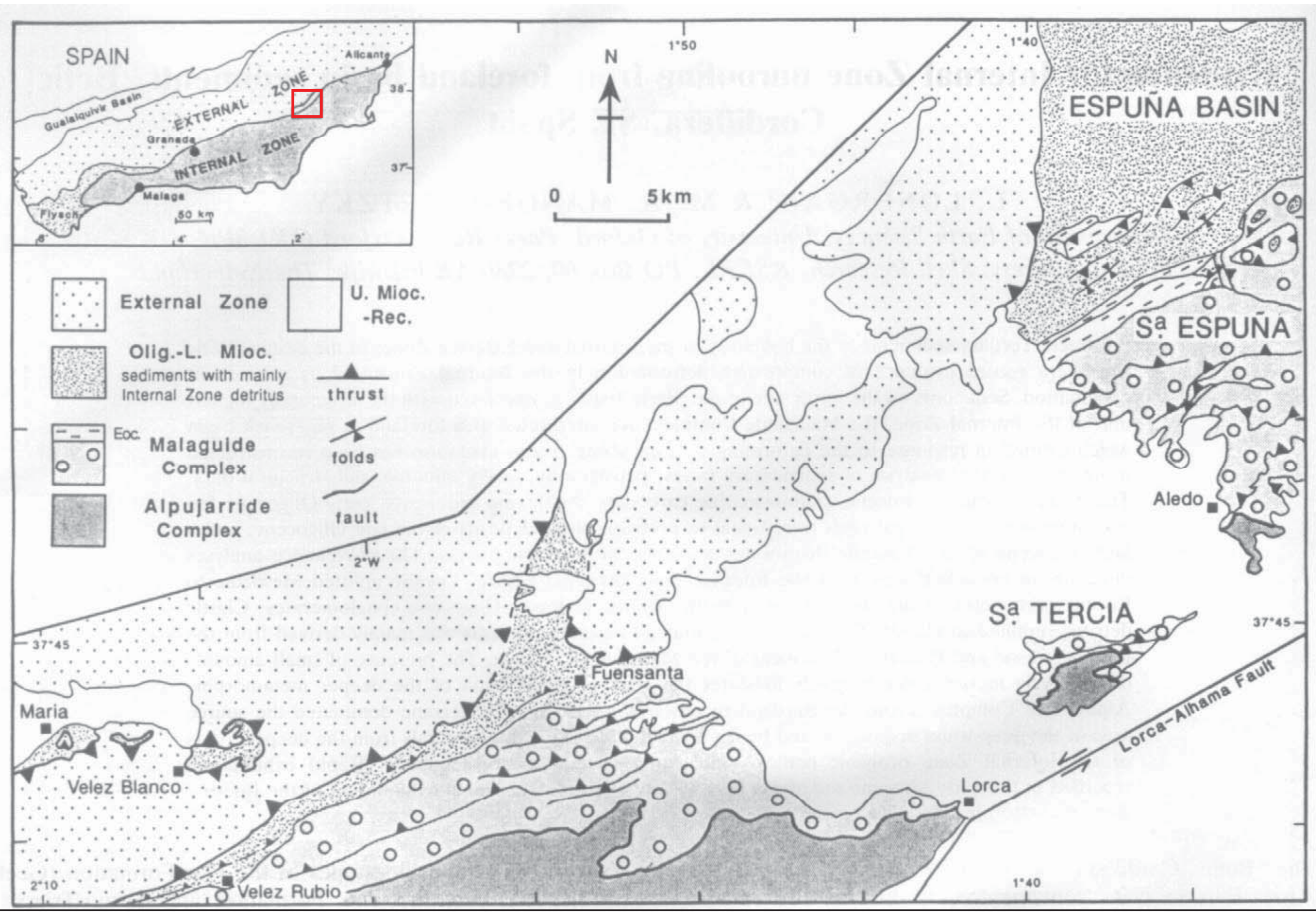

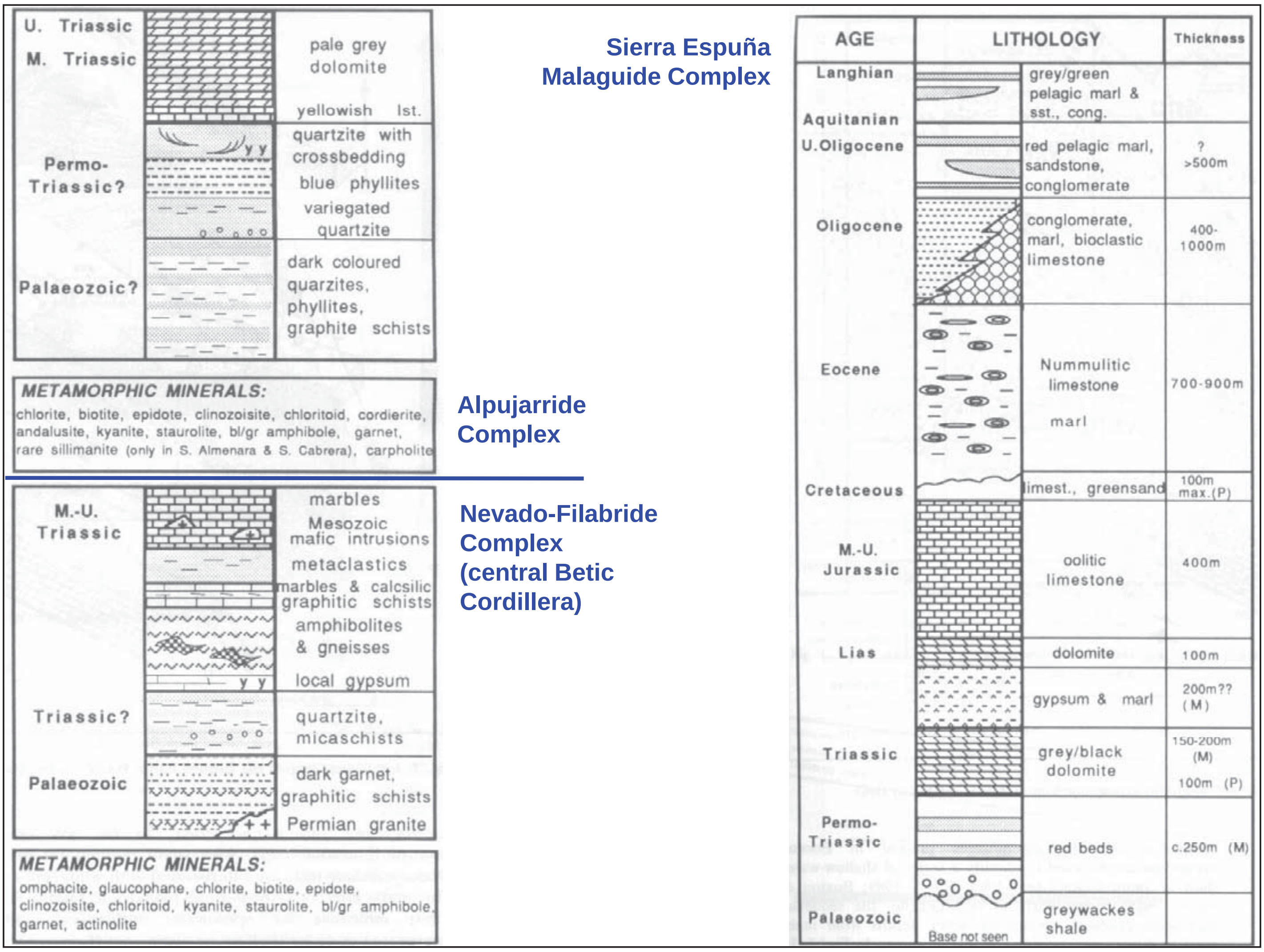

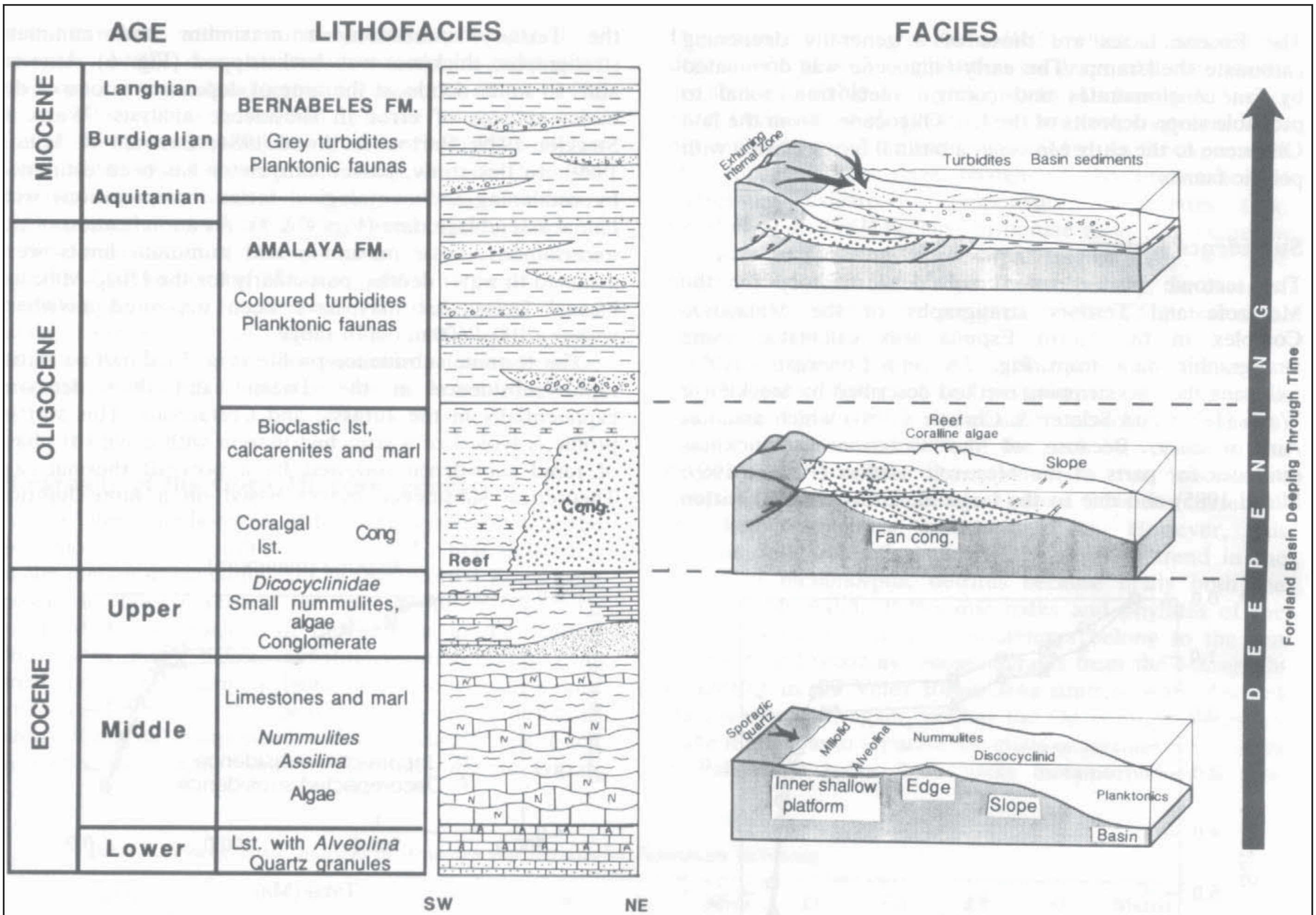

Fig. 4. Facies summary of the Espuña foreland basin, illustrating a generally deepening sequence through time.

Subsidence Analysis

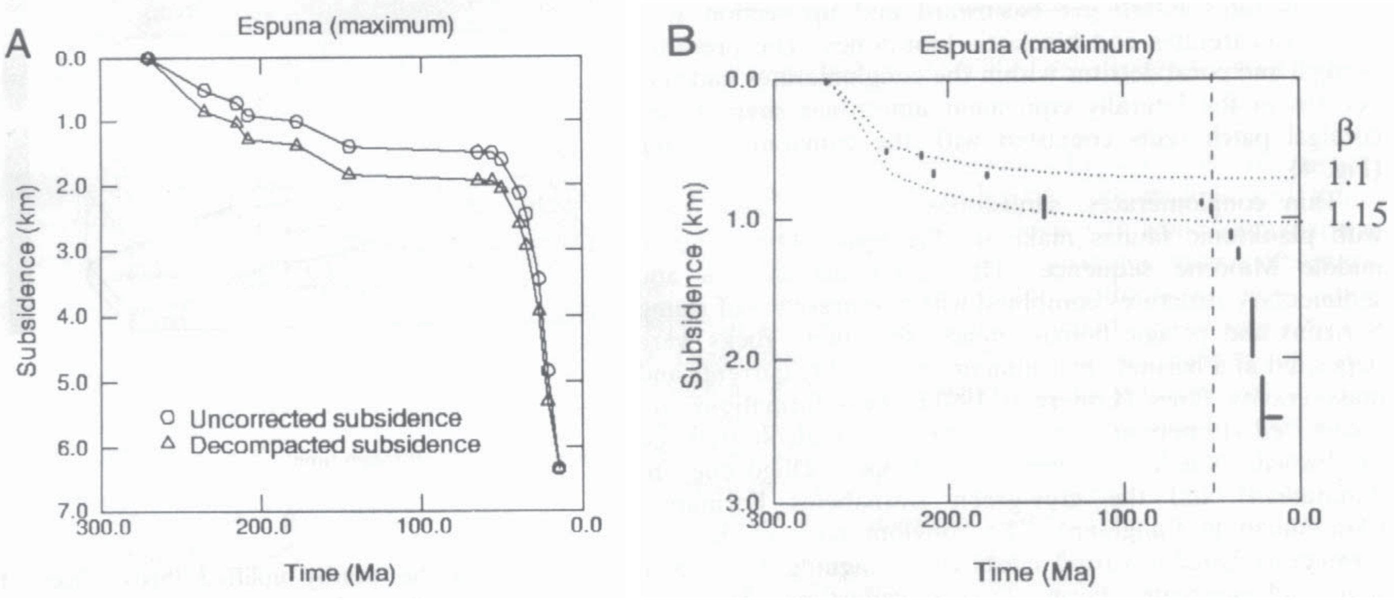

Fig. 6. Subsidence analysis for a maximum and minimum thickness of the España Malaguide section: (**A**) Circles, uncorrected subsidence; triangles, decompacted subsidence. (**B**) Vertical bars, water-loaded or tectonic subsidence including uncertainty in palaeowater depth. The effect of sediment loading has been removed by replacing the sediment with water and assuming Airy isostasy. Dotted lines are best-fitting maximum and minimum theoretical subsidence curves for a rift basin with finite duration stretching with uniform strain rates, and an initial crustal thickness of 30 km. Vertical dashed line indicates significant departure of observed subsidence from the theoretical rift model. At the start of the Tertiary (65–50 Ma) there is a rapid increase in subsidence due to the onset of foreland basin development.

Petrographic composition

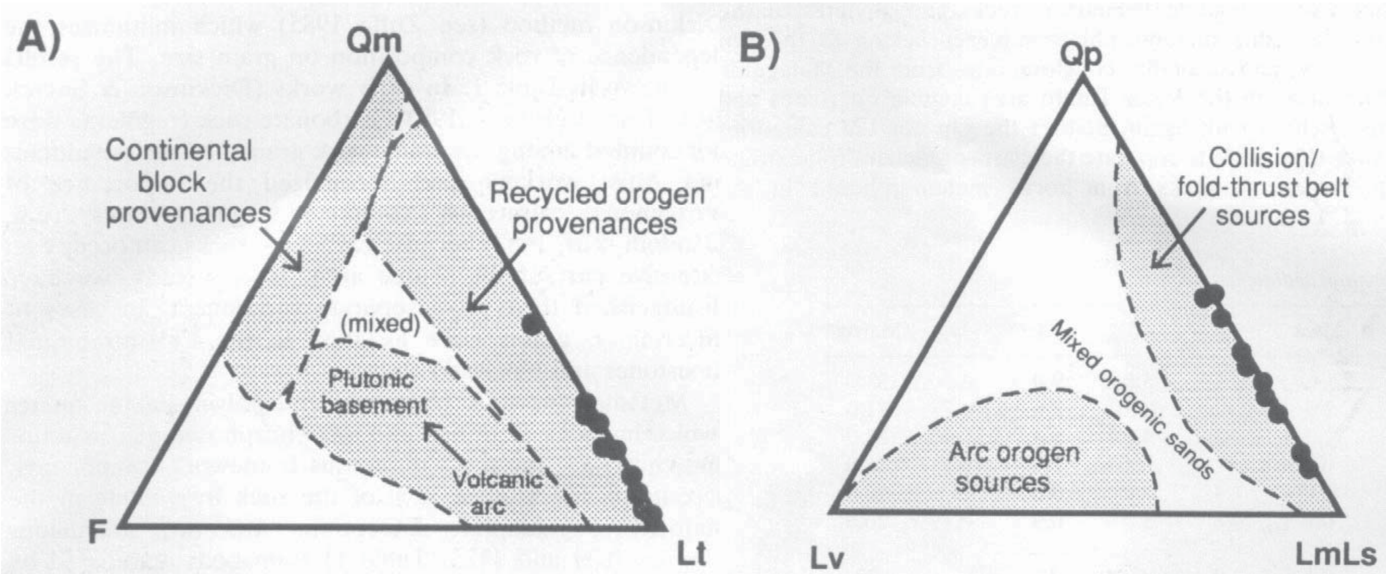

Fig. 7. Sandstones from the Amalaya and Bernabeles Formations plotted on Q_m,F,L_t (**A**) and Q_p,L_v,L_m,L_s (**B**) triangular diagrams, using framework petrology data from Table 1. The sandstones fall within the recycled orogen and collisional fold and thrust belt fields when compared with the actual distribution of mean detrital modes of recent sandstone suites (shaded fields on the triangle plots, from Dickinson 1985).

Heavy Minerals

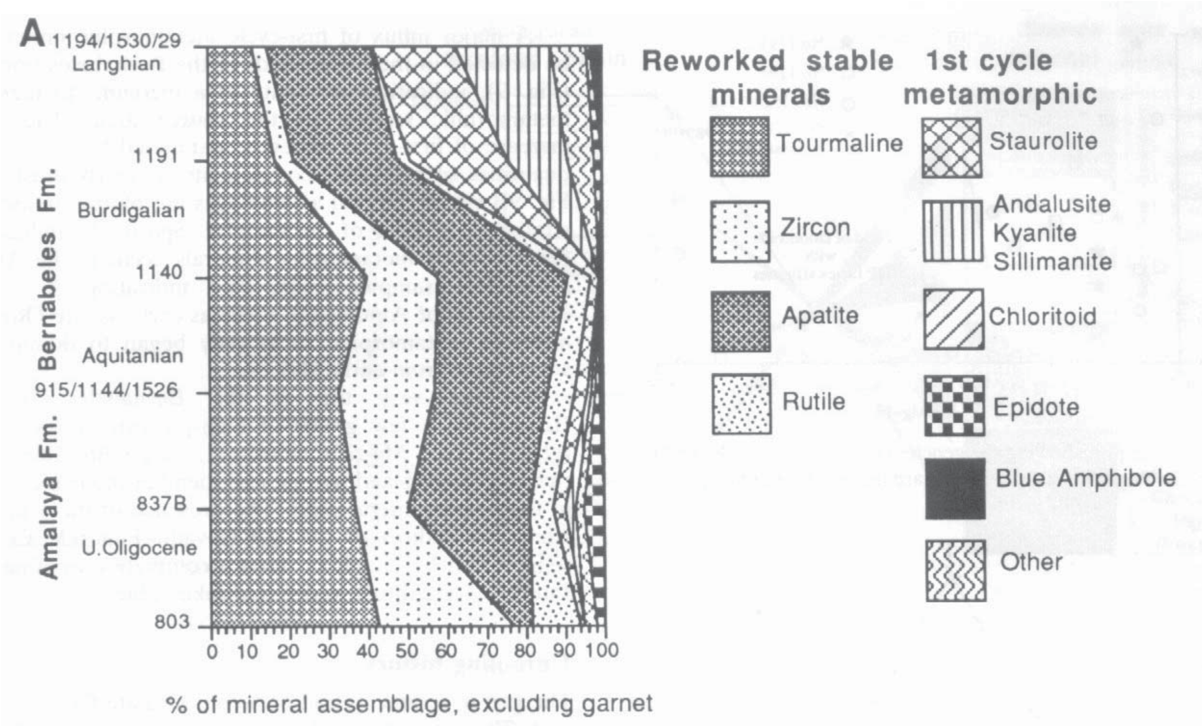

Fig. 9. (**A**) Results of heavy mineral analyses arranged in ascending stratigraphic order. Reworked stable minerals were derived from the Malaguide Complex, whereas first-cycle metamorphic minerals were derived from the Alpujarride and Nevado-Filabride Complexes. (**B**) Summary plots illustrating the main trends of heavy mineral composition in the upper Oligocene and Miocene stratigraphic section. Plot (a) illustrates the Internal Zone unroofing history with reworked stable minerals eroded from the highest sedimentary rocks dominating the lowest part of the section. A major influx of metamorphic minerals occurs in the Burdigalian, and high-pressure (*HP*) index minerals from the structurally lowest Nevado-Filabride Complex appear at the top of the section in the Langhian. Plot (b) illustrates the accompanying increase of garnets. Ratios of stable reworked (tourmaline, zircon, rutile and apatite) to metamorphic minerals are presented in plot (c).

Heavy Minerals

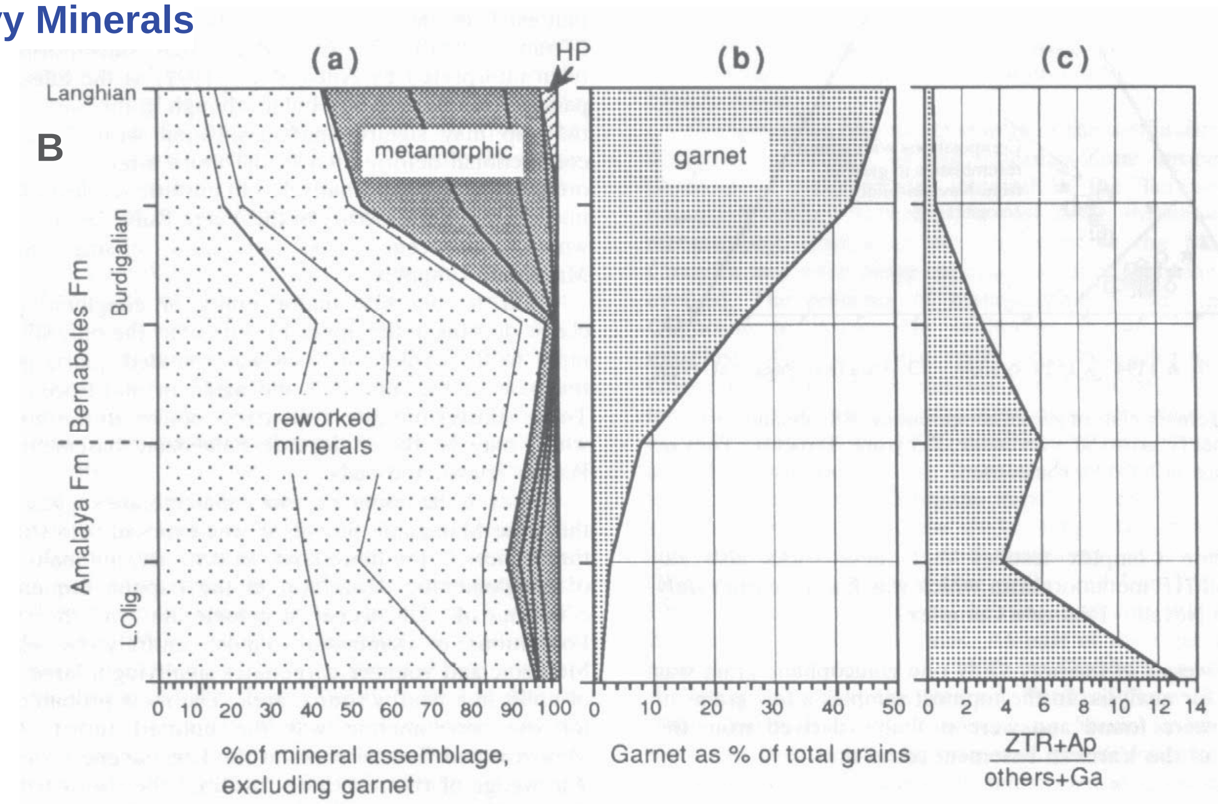

Fig. 9. (**A**) Results of heavy mineral analyses arranged in ascending stratigraphic order. Reworked stable minerals were derived from the Malaguide Complex, whereas first-cycle metamorphic minerals were derived from the Alpujarride and Nevado-Filabride Complexes. (**B**) Summary plots illustrating the main trends of heavy mineral composition in the upper Oligocene and Miocene stratigraphic section. Plot (a) illustrates the Internal Zone unroofing history with reworked stable minerals eroded from the highest sedimentary rocks dominating the lowest part of the section. A major influx of metamorphic minerals occurs in the Burdigalian, and high-pressure (*HP*) index minerals from the structurally lowest Nevado-Filabride Complex appear at the top of the section in the Langhian. Plot (b) illustrates the accompanying increase of garnets. Ratios of stable reworked (tourmaline, zircon, rutile and apatite) to metamorphic minerals are presented in plot (c).

Chloritoid chemistry

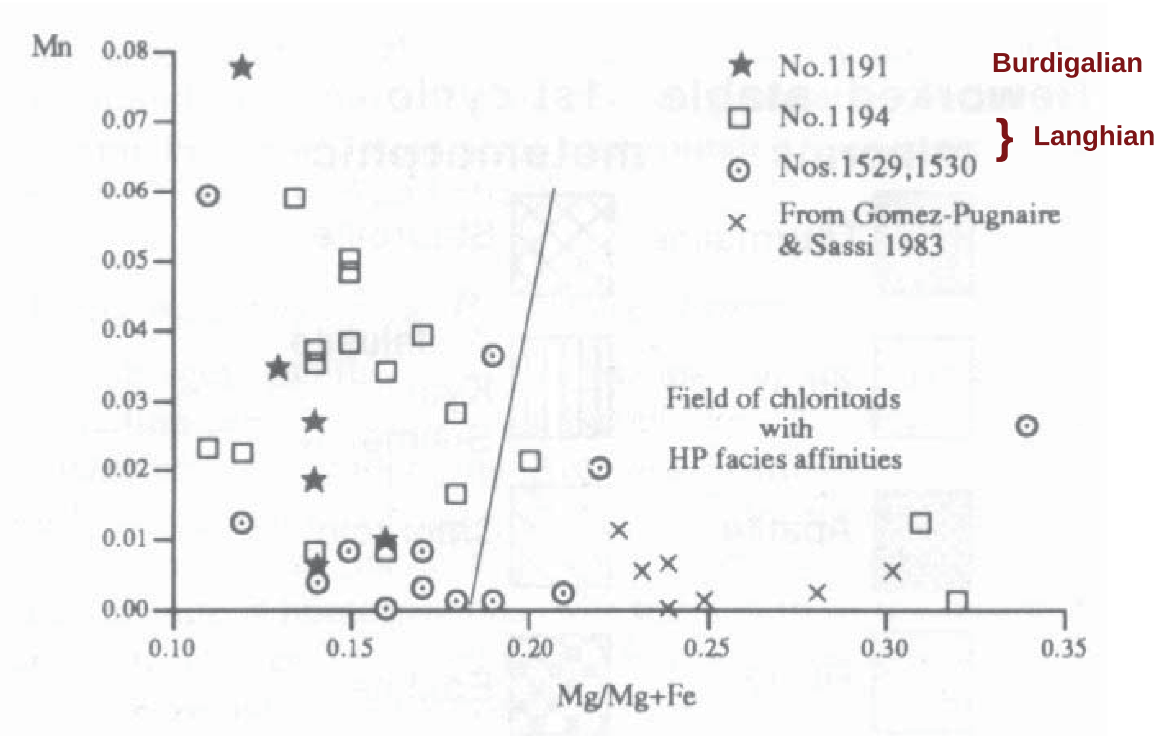

Fig. 10. Scatter plot showing the geochemistry of chloritoids. Data from Gomez-Pugnaire & Sassi (1983) are included for comparison.

Summary Oligocene/Miocene Betic Cordillera

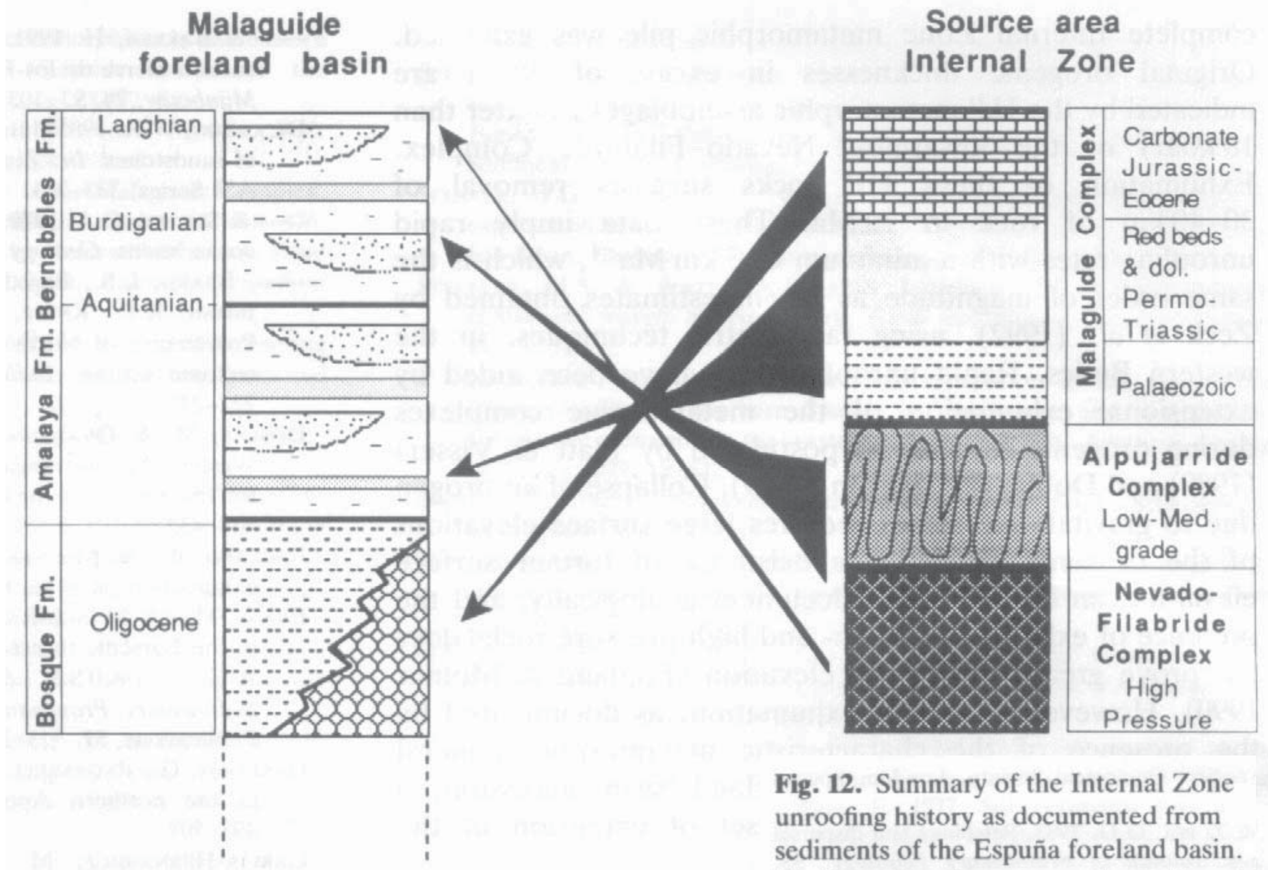

Fig. 12. Summary of the Internal Zone unroofing history as documented from sediments of the Espuña foreland basin. Stratigraphic columns are schematic and not to scale.